



## An ecologically-constrained deep learning model for tropical leaf phenology monitoring using PlanetScope satellites



Jing Wang <sup>a,b,1</sup>, Guangqin Song <sup>b,1</sup>, Michael Liddell <sup>c</sup>, Patricia Morellato <sup>d</sup>, Calvin K.F. Lee <sup>b</sup>, Dedi Yang <sup>e</sup>, Bruna Alberton <sup>d,f</sup>, Matteo Detto <sup>g</sup>, Xuanlong Ma <sup>h,i,j</sup>, Yingyi Zhao <sup>b</sup>, Henry C.H. Yeung <sup>b</sup>, Hongsheng Zhang <sup>k,l</sup>, Michael Ng <sup>m</sup>, Bruce W. Nelson <sup>n</sup>, Alfredo Huete <sup>o</sup>, Jin Wu <sup>b,1,\*</sup>

<sup>a</sup> School of Ecology, Shenzhen Campus of Sun Yat-sen University, Shenzhen, Guangdong, China

<sup>b</sup> Research Area of Ecology and Biodiversity, School for Biological Sciences, The University of Hong Kong, Hong Kong, China

<sup>c</sup> Centre for Tropical Environmental and Sustainability Science, College of Science and Engineering, James Cook University, Cairns, Queensland 4878, Australia

<sup>d</sup> Department of Biodiversity, Bioscience Institute, São Paulo State University UNESP, Rio Claro, São Paulo, Brazil

<sup>e</sup> Department of Environmental and Climate Sciences, Brookhaven National Laboratory, NY11973, USA

<sup>f</sup> Instituto Tecnológico Vale, Belém, Pará, Brazil

<sup>g</sup> Department of Ecology and Evolutionary Biology, Princeton University, Princeton, NJ 08544, USA

<sup>h</sup> College of Earth and Environmental Sciences, Lanzhou University, Lanzhou, China

<sup>i</sup> International Research Center of Big Data for Sustainable Development Goals, Beijing, China

<sup>j</sup> Key Laboratory of Geographic Information Science (Ministry of Education), East China Normal University, Shanghai, China

<sup>k</sup> Department of Geography, The University of Hong Kong, Hong Kong, China

<sup>l</sup> Institute for Climate and Carbon Neutrality, The University of Hong Kong, Hong Kong, China

<sup>m</sup> Institute of Data Science and Department of Mathematics, The University of Hong Kong, Hong Kong, China

<sup>n</sup> National Institute for Amazon Research (INPA), Manaus, Brazil

<sup>o</sup> School of Life Sciences, University of Technology Sydney, Sydney, NSW 2007, Australia

### ARTICLE INFO

Edited by Marie Weiss

#### Keywords:

Tropical forests  
Carbon cycles  
Environmental gradient  
Deciduousness  
Multi-scale remote sensing  
Machine learning

### ABSTRACT

In tropical forests, leaf phenology signals leaf-on/off status and exhibits considerable variability across scales from a single tree-crown to the entire forest ecosystem. Such phenology signals importantly regulate large-scale biogeochemical cycles and regional climate. PlanetScope CubeSats data with a 3-m resolution and near-daily global coverage provide an unprecedented opportunity to monitor both fine- and ecosystem-scale phenology variability along large environmental gradients. However, a scalable method that accurately characterizes leaf phenology from PlanetScope with biophysically meaningful metrics remains lacking. We developed an index-guided, ecologically constrained autoencoder (IG-ECAE) method to automatically derive a deciduousness metric (percentage of upper tree canopies with leaf-off status within an image pixel) from PlanetScope. The IG-ECAE first estimated the reflectance spectra of leafy/leafless canopies based on their spectral indices characteristics, then used the derived reflectance spectra to guide an autoencoder deep learning method with additional ecological constraints to refine the reflectance spectra, and finally used linear spectral unmixing to estimate the relative abundance of leafless canopies (or deciduousness) per PlanetScope image pixel. We tested the IG-ECAE method at 16 tropical forest sites spanning multiple continents and a large precipitation gradient (1470–2819 mm year<sup>-1</sup>). Among these sites, we evaluated the PlanetScope-derived deciduousness against corresponding measures derived from WorldView-2 ( $n = 9$  sites) and local phenocams ( $n = 9$  sites). Our results show that PlanetScope-derived deciduousness agrees: 1) with that derived from WorldView-2 at the patch level (90 m × 90 m) with  $r^2 = 0.89$  across all sites; and 2) with that derived from phenocams to quantify ecosystem-scale seasonality with  $r^2$  ranging from 0.62 to 0.96. These results demonstrate the effectiveness and scalability of IG-ECAE in characterizing the wide variability in deciduousness across scales from pixels to forest ecosystems, and from a

\* Corresponding author at: School for Biological Sciences, The University of Hong Kong, Pokfulam Road, Hong Kong, China.

E-mail address: [jinwu@hku.hk](mailto:jinwu@hku.hk) (J. Wu).

<sup>1</sup> Equal contribution.

single date to the full annual cycle, indicating the potential for using high-resolution satellites to track the large-scale phenological patterns and response of tropical forests to climate change.

## 1. Introduction

Tropical leaf phenology controls vegetation feedback to regional climate systems by influencing the seasonal and spatial variability in carbon, water, and energy fluxes (Beer et al., 2010; Wright et al., 2017; Xu et al., 2020). Due to year-round warm and seasonally moist environments, tropical landscapes often harbor the highest diversity of woody plant species. This taxonomic diversity is reflected in a plethora of leaf phenology strategies adapted to and competitive for various resources of light, water, and nutrients (Dettlo et al., 2018; Vanschaik et al., 1993; Xu et al., 2017). Such high diversity in leaf phenology strategies is often observed at both ecosystem and fine (i.e. individuals/species) scales. At the ecosystem scale, tropical leaf phenology shows a wide variation in seasonal patterns across environmental gradients (Guan et al., 2015; Satake et al., 2022). At the fine scale, leaf phenology of individual trees or species within the same forest community often varies in their seasonal displays, ranging from individuals that exchange leaves multiple times per year to those that slowly turnover only once in several years (Alberton et al., 2014; de Camargo et al., 2018; Dettlo et al., 2018; Reich, 1995). Such diverse phenological strategies at the fine scale collectively shape community assemblage, and determine ecosystem-scale phenology patterns and many phenology-related ecosystem functions and services (Forzieri et al., 2020; Morellato et al., 2016; Renner and Zohner, 2018). However, as reported by many field- and proximate remote sensing studies (Blanchard et al., 2016; Panzou et al., 2021; Park et al., 2019), >50% of tropical tree-crowns have crown diameters <10 m but larger than 3 m. Ground inventory and proximal remote sensing (e.g. tower-based phenocam measurements, frequent drone flights) are able to resolve individual tree-crown scale phenological monitoring but are constrained by the limited spatial coverage, while traditional satellite remote sensing observations (e.g. Moderate Resolution Imaging Spectroradiometer, MODIS of 500 m per pixel, Landsat of 30 m, and Sentinel-2 of 10 m) was limited due to the coarser spatial resolution. Therefore, accurate characterization and scalable tracking of changes in tropical leaf phenology from the fine- to ecosystem-scale remains challenging.

The recent launch of new-generation satellites with high spatial and temporal resolutions offers a novel opportunity to advance cross-scale leaf phenology monitoring while addressing observational limitations inherent in traditional ground/proximate/satellite methods. For example, the PlanetScope constellation of 180+ CubeSats provides near-daily global coverage at a 3-m spatial resolution and has been demonstrated as a promising alternative for leaf phenology monitoring across various scales (Moon et al., 2021; Wang et al., 2020; Wu et al., 2021). While PlanetScope data are subject to artifacts associated with the cloud/cloud shadow contamination, Bidirectional Reflectance Distribution Function (BRDF) effect, and radiometric calibration inconsistencies among the different PlanetScope sensors, a series of methods have been developed to minimize these artifacts. For example, to minimize cloud/cloud shadow contamination, Wang et al. (2021) developed a spatiotemporal integration method for automatic cloud and shadow screening, demonstrating consistently high accuracy and scalability across representative tropical landscapes. To minimize the BRDF effect and address the cross-sensor inconsistency issue, Houborg and McCabe (2018a, 2018b) and Wang et al. (2020) developed cross-sensor calibration methods with demonstrated improvements in the data quality and consistency across both space and time. With these methodological advances and improved data quality, the use of PlanetScope is increasingly suggested as an important way forward to advance cross-scale phenology monitoring in the tropics.

With few site-level studies suggesting the potential of using PlanetScope for cross-scale phenology characterization (Chen et al., 2019;

Moon et al., 2021; Wang et al., 2020; Wu et al., 2021), the time is ripe for developing a scalable method that accurately characterizes leaf phenological patterns with biophysically meaningful metrics across large tropical landscapes. Remotely sensed spectral vegetation indices (VIs) like normalized difference vegetation index (NDVI), enhanced vegetation index (EVI), and green chromatic coordinate (GCC) have been widely used for leaf phenology characterizations over large tropical areas (Alberton et al., 2019; Gonçalves et al., 2020; Huete et al., 2006; Huete et al., 2008; Ma et al., 2013; Maeda et al., 2016), but the biophysical meaning of these metrics remains unclear (Brando et al., 2010; Lopes et al., 2016; Song et al., 2022; Wagner et al., 2017; Wu et al., 2018). For example, VIs are sensitive to both the leaf age demography and leaf cover of the upper forest canopy (Wu et al., 2018). This ambiguity complicates the mechanistic interpretation between seasonal variations in VIs and the phenology of leaf age and leaf cover. To address this challenge, Park et al. (2019) and Song et al. (2022) used a leaf fraction metric, the proportion of all leaves within a given tree crown, to quantify tropical leaf phenology using proximate remote sensing data, such as phenocam and drone observations. Wang et al. (2020) used non-photosynthetic vegetation abundance, a deciduousness metric (1- leaf fraction) indicating the percentage of upper tree canopies with leaf-off status for each PlanetScope pixel, to help quantify leaf phenology variability across scales from a 3-m image pixel to the entire forest ecosystem. Despite initial successes of this method, the method has only been tested at limited tropical forest sites and it is unclear whether it can be extended to other regions of the tropics.

The methods to accurately derive a deciduousness metric (i.e. the percentage of upper tree canopies with leaf-off status within an image pixel) from satellite images can be broadly classified into two categories: spectral unmixing (e.g. Adams et al., 1995; Asner et al., 2009) and machine learning-based methods (e.g. Bhattacharai et al., 2021; Host et al., 2020; Huechacona-Ruiz et al., 2020). Spectral unmixing methods assume that the reflectance spectrum of an image pixel is a combination of spectral constituents (i.e. reflectance spectra of endmembers) weighted by their abundance within the pixel (Keshava and Mustard, 2002). These methods usually include two steps: 1) endmember extraction either from 'pure' image pixels fully occupied by one of the constituents (e.g. fully leafy or leafless tree canopies in our case) or field-based spectral library, and 2) abundance estimation using the spectral unmixing analysis (Adams et al., 1995; Asner et al., 2009; Shimabukuro and Smith, 1991). Machine learning-based methods, such as random forest, support vector machine, and artificial neural network (Host et al., 2020; Huechacona-Ruiz et al., 2020; Laurin et al., 2016), rely on large sets of training samples to calibrate complex models for abundance mapping, and have been used on hyperspectral images and Sentinel-2 images (Host et al., 2020; Laurin et al., 2016). As large training samples across various environmental gradients, forest types, and seasons are needed, this kind of methods is less scalable unless a very comprehensive training dataset is built up across the various axes of natural variability.

Despite these two categories of methods having been widely used in the remote sensing field for various applications, their capacity to characterize leaf phenology using PlanetScope data across large and diverse tropical landscapes remains unknown. For spectral unmixing methods, the endmember spectra often vary largely across different forest sites due to the variation in species compositions, canopy structure, and environmental conditions (Somers et al., 2011; Zare and Ho, 2014). While most machine learning methods typically have very limited scalability when moving from one site with intensive training samples to other more diverse sites without further collection of training samples. In this study, we assume that integrating spectral unmixing with machine learning-based methods may provide a more scalable and

reliable approach for deciduousness mapping. The underlying reason is that using an appropriate machine learning method could aid the automatic extraction of endmember spectra to resolve the bias and noise from endmember variability across large landscapes, while spectral unmixing would help derive the deciduousness metric effectively at the pixel level without any prior training requirements. This reasoning seems to be supported by evidence from previous studies in other fields using machine learning-based spectral unmixing methods (Dopido et al., 2012; Han et al., 2021; Min et al., 2021; Xu et al., 2019). For example, Min et al. (2021) and Han et al. (2021) developed autoencoder-based spectral unmixing methods and found these methods would not only enable the automatic extractions of pure endmember spectra without any prior training samples as input, but also demonstrated improvements in accuracy in the abundance mapping of vegetation, soil, and buildings (Dopido et al., 2012; Xu et al., 2019). However, their methods were found to have large uncertainties, mainly associated with the initialization of the endmember extraction and the simple optimization discipline (e.g. minimizing the difference between modeled and observed reflectance spectra) that would lead to the extracted endmembers without a clear biophysical meaning. To address these issues, candidate solutions could be to leverage remotely sensed spectral indices to guide the endmember extractions (Deng and Wu, 2013; Sun et al., 2016) or incorporate prior knowledge-based constraints (e.g. ecological constraints) to improve automatic endmember extraction accuracy (Qu and Qi, 2019). However, the comprehensive assessments of the effectiveness and scalability of this integrated method (e.g. spectral indices plus autoencoder-based spectral unmixing) with or without ecological constraints for large-scale tropical deciduousness mapping using PlanetScope data remain under-explored.

The goal of this study is to explore a novel integrated method (i.e. index-guided, ecologically constrained autoencoder; or IG-ECAE) for cross-scale deciduousness monitoring using PlanetScope satellite data across large environmental gradients in the tropics. We expect this integrated method to resolve the scalability concern as it offers a more accurate and automatic way to characterize endmember variability that is challenging for traditional spectral unmixing methods, while reducing the intensive labor involved in traditional machine learning-based methods. There are three key steps in this IG-ECAE method: 1)

identifying candidate endmembers representing fully leafy, fully leafless, and fully shaded pixels based on their characteristics in remote sensing derived spectral indices, 2) determining site-specific “true” endmembers using the above-derived candidate endmembers to guide an autoencoder-based machine learning method, which is subject to important ecological constraints following prior knowledge of the spectral characteristics of endmembers, and 3) estimating the abundance of leafless canopies (i.e. deciduousness) using linear spectral unmixing analysis. As a proof-of-concept, we selected 16 preserved forest sites spanning a large gradient in mean annual precipitation and deciduous character across multiple continents in the tropics.

## 2. Study sites and materials

### 2.1. Study sites

We selected 16 tropical sites (Fig. 1) representative of preserved forests across five continents and spanning large environmental gradients, including North America ( $n = 3$ ), South America ( $n = 6$ ), Africa ( $n = 2$ ), Asia ( $n = 3$ ), and Oceania ( $n = 2$ ). Details regarding the location, climate, and dry seasons of these sites are shown in Table 1.

These sites were selected for three reasons. First, there were independent observations made at these sites, including high spatial resolution WorldView-2 ( $n = 9$  sites) and/or tower-based phenocam images ( $n = 9$  sites, including 2 overlapping sites) (Table 1). Second, these sites represent distinct forest communities with varying abundances of evergreen and deciduous trees, and span a large precipitation gradient (mean annual precipitation: 1470–2819 mm) and dry season length (the number of months with precipitation lower than 100 mm: 0–12 months per year). For example, the Palo Verde National Park site (henceforth ‘01-PVNP’) is a tropical dry forest landscape from Guanacaste in Costa Rica containing up to 80% tree canopies of deciduous species (Arroyo-Mora et al., 2005), while the Pasoh Forest Reserve site (henceforth ‘12-Pasoh’) is a tropical moist forest landscape from Negeri Sembilan in Malaysia almost fully covered by evergreen tree species (Kochummen et al., 1990). Third, these sites have rich plant diversity and include vast variability in leaf phenology patterns across scales from single tree crowns up to forest ecosystems. For example, the four tropical evergreen

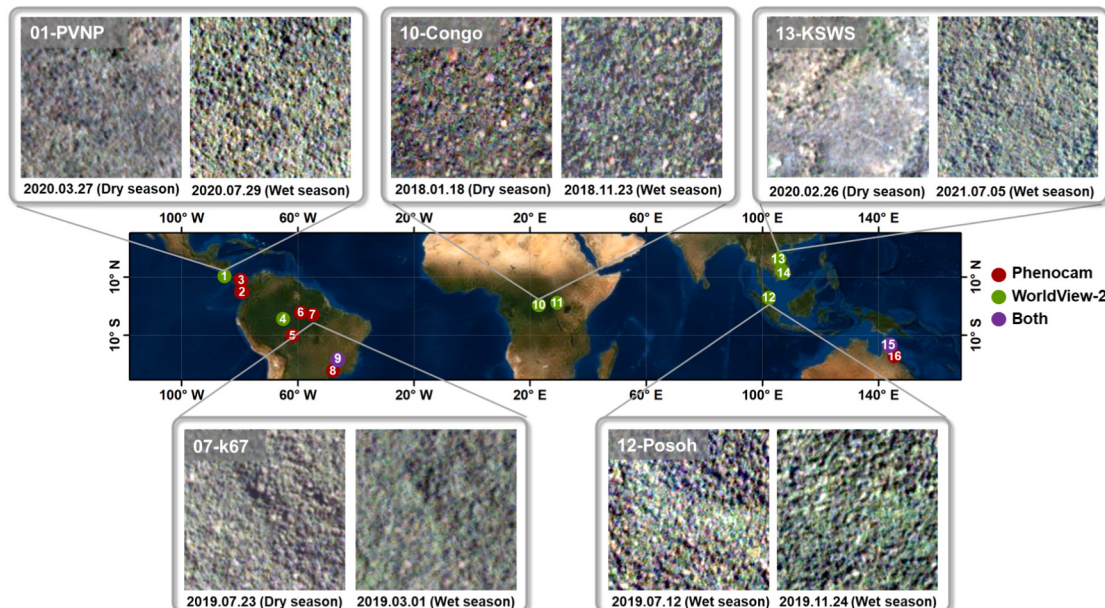


**Fig. 1.** Study sites where PlanetScope images were matched to WorldView-2 and/or Phenocam data. Red circles indicate the nine sites with phenocams, green circles indicate the nine sites with WorldView-2 images, and purple circles indicate the sites with both phenocams and WorldView-2 images. PlanetScope image pairs from local dry and/or wet seasons are shown for five sites. (For interpretation of the references to colour in this figure legend, the reader is referred to the web version of this article.)

**Table 1**  
Detailed information of the sixteen testing sites.

Site ID	Site name	Country	Latitude/ Longitude	MAP (mm year <sup>-1</sup> )	DSL (months)	PS availability	No. of PS images	Phenocam availability	WorldView-2 availability
01-PVNP	Palo Verde National Park	Costa Rica	10.37°N/85.34°W	2102(1817)	5	2020	12	03/2013–05/2017 12/2016–12/2017	3/29/2020
02-BCI	Panama BCI	Panama	9.15°N/79.85°W	2441(2662)	4	2018–2020	81		
03-PNM	Panama PNM	Panama	8.99°N/79.54°W	1913	4	2020	93		
04-AMZ	Amazon Forest	Brazil	4.38°S/65.14°W	2819	0	2020	16		7/21/2020
05-RJA	Reserva Jaru	Brazil	10.08°S/61.93°W	1880	5	2018–2020	107	12/2017–12/2018	
06-ATTO	Manaus ATTO	Brazil	2.14°S/59.00°W	2345(2300)	2	2018–2020	64	07/2013–12/2014	
07-k67	Tapajos k67	Brazil	2.85°S/54.97°W	1964(1700)	5	2018–2020	57	01/2010–12/2011	
08-Core	Cerrado Core	Brazil	22.18°S/47.87°W	1481	6	2018–2019	170	01/2018–12/2019	
09-PEG	Cerrado PEG	Brazil	21.63°S/47.63°W	1470	6	2018–2019, 2021	283	01/2018–06/2018 ; 08–2019–12/2019	3/25/2021
10-Congo	Congo	Africa	0.42°N/23.09°E	1947	1	2019	11		4/1/2019
11-NCongo	North of Congo	Africa	1.24°N/29.36°E	1563	3	2018	25		9/7/2018
12-Pasoh	Pasoh Forest	Malaysia	2.99°N/102.31°E	2225(1842)	0	2019	10		7/11/2019
13-KSWS	Keo Seima Wildlife Sanctuary	Thailand	12.44°N/106.89°E	2243	4	2020	15		2/25/2020
14-NAM	Nam Cat Tien	Vietnam	11.49°N/107.40°E	2665	4	2020	17		2/14/2020
15-CowB	Cow Bay	Australia	16.10°S/145.43°E	1515(3700)	7	2018–2019	36	01/2018–12/2018	8/11/2019
16-RobC	Robson Creek	Australia	17.12°S/145.63°E	1598(2264)	7	2018	46	01/2018–12/2018	

MAP: mean annual precipitation; MAP value is assessed from the Tropical Rainfall Measuring Mission (TRMM) data from 2000 to 2019. Brackets values in the column of MAP show the site observations. DSL: dry season length; PS: PlanetScope.

forest sites located in the Brazilian Amazon, i.e. Western Amazonas forest ('04-AMZ'), southern forest of Reserva Jaru ('05-RJA'), Amazon Tall Tower Observatory ('06-ATTO'), and Tapajos National Forest k67 ('07-k67'), exhibit modest to large seasonal reflectance variability caused by different leaf phenology patterns of tree species at the tree-crown scale, ranging from evergreen to semi-deciduous and fully deciduous (Lopes et al., 2016; Wu et al., 2016). For more details about the ecological, hydrological, and topographic characteristics of these sites, please refer to previous studies (Alberton et al., 2019; Arroyo-Mora et al., 2005; Blanc et al., 2000; Ifo et al., 2016; Knight, 1975; Kochummen et al., 1990; Moore et al., 2016; Wu et al., 2016).

## 2.2. Materials

We used four types of data in this study: tower-based phenocams, and three types of optical satellite remote sensing (WorldView-2, PlanetScope, and MODIS). The four types of input data are described in detail below:

(1) Phenocam images. Three-band RGB (red, green, and blue) phenocams were mounted on local towers for leaf phenology monitoring at 9 tropical forest sites (Fig. 1; more details regarding the RGB images and phenocam orientations refer to Fig. S1 and Table S1). These phenocams covered upper canopy tree-crowns (from 12 to 267; Table S1) within each image of the forest landscape, and were programmed for automatic image acquisition every 10–30 min during daytime over a few years (1–5 years). Details regarding the temporal coverage of these phenocams and others can refer to Table 1 and previous publications (Alberton et al., 2014; Alberton et al., 2019; Liddell and Weigand, 2021; Moore et al., 2016; Wu et al., 2016). With these phenocam data, we then turned to a crown-cased phenology inventory approach (Wu et al., 2016). Specifically, we first manually selected the best quality image every 6 days throughout the entire image time series. We then labelled all individual well-illuminated tree-crowns in the phenocam view and visually assigned each crown to one of two phenophases: leafless (leaf shedding or bare branch materials accounts for around or >50% of the entire tree crown area) or leafy (otherwise), based on their colors, textures and temporal trends of leaf colour within the adjacent two weeks. Finally, for each selected image, we calculated the deciduousness metric by dividing the number of leafless tree-crowns by all identified tree-crowns. A mean annual cycle of monthly deciduousness was derived to indicate ecosystem-scale seasonality of deciduousness which was subsequently used as the ground truth to validate the deciduousness seasonality derived from PlanetScope satellite data.

(2) WorldView-2 surface reflectance products. WorldView-2 data have one panchromatic band at a 0.5-m spatial resolution and eight spectral bands (400–1040 nm) at 1.8-m spatial resolution. These data were accessed from <https://discover.digitalglobe.com/> through a contract with MAXAR (Westminster, CO). We surveyed all available WorldView-2 data from 2018 to 2021 over our study sites and selected the clearest images with low cloud cover (<10% via visual assessment, mostly distributed in the dry season), resulting in a total of 9 available images (Fig. 1) with one image per site, each covering a 5 km × 5 km area. See Table 1 for acquisition dates. The Standard Level 2A surface reflectance product was used in this study, as it has been orthorectified, geo-referenced, and radiometrically and atmospherically corrected (DigitalGlobe, 2021). The product was first used to map the spatial variability in forest deciduousness both within and across sites (see Section 3.1 below), and then used as a benchmark to evaluate the agreement with deciduousness derived from PlanetScope.

(3) PlanetScope surface reflectance products. Four-band (blue, green, red, and near-infrared (NIR)) PlanetScope data with a 3-m spatial resolution from Planet Labs PBC (San Francisco, CA, USA) were used in this study. The data were accessed from <https://www.planet.com/> through a research and education license. The level 3B surface reflectance product of PlanetScope was used in this study, which has been orthorectified and preprocessed, including geometric, radiometric, and

atmospheric corrections (Planet, 2022). Since the above phenocams and WorldView-2 data varied considerably in their temporal availability across forest sites (Table 1), we accordingly obtained the time-series PlanetScope data that covered the same year as phenocam and/or WorldView-2 data. For certain sites, phenocam data had a temporal coverage beyond the focused coverage of PlanetScope (2018–present), we thus assessed the full-year PlanetScope data in 2018–2020 and used the averaged deciduousness seasonality for evaluation (Table 1). Consequently, a total of 1043 daily images of PlanetScope with low cloud cover (<40%) were used in this study.

(4) MODIS surface reflectance products. The coarse-resolution MODIS data were used in this study for cross-calibrating PlanetScope satellite data to address the cross-sensor radiometric inconsistency issue and variable view and illumination geometries of PlanetScope observations. Specifically, the daily MODIS BRDF/Albedo model parameter product, MCD43A1 (Schaaf et al., 2002), at a 500-m resolution from January 2016 to December 2021 was accessed at <http://ladsweb.nascom.nasa.gov/> and used in this study. With this data, we first adjusted it to simulate a fixed sun-sensor geometry (nadir view and solar zenith angle of 45°) (Morton et al., 2014; Saleska et al., 2016), and then used the BRDF-adjusted MODIS data to cross-calibrate PlanetScope data following the approach of Wang et al. (2020).

Notably, as this study focused on leaf phenology monitoring in preserved tropical forests, we manually masked out non-forest areas (e.g. water bodies, bare soil, buildings, and roads) from the satellite images at six sites (i.e. 02-BCI, 03-PNM, 08-Core, 12-Posoh, 14-NAM, and 15-CowB).

### 3. Methods

To evaluate the potential of using PlanetScope data for cross-scale phenology monitoring over large tropical areas, we divided the work into four tasks (Fig. 2): 1) estimating the deciduousness metric from WorldView-2 data using a random forest (RF)-based classification method; 2) pre-processing PlanetScope data to minimize potential impacts caused by cloud and cloud shadow contamination, BRDF effect, and cross-sensor inconsistency inherent in PlanetScope data; 3) estimating the deciduousness metric from PlanetScope data using IG-ECAE; and 4) evaluating the accuracy and scalability of PlanetScope-derived deciduousness metric against the correspondences derived from WorldView-2 and/or phenocam images.

#### 3.1. Estimating the deciduousness metric from WorldView-2 data

In order to derive an accurate benchmark of deciduousness metric for evaluating the corresponding metric derived from PlanetScope, we performed a RF-based supervised classification at pixel level for each WorldView-2 image. The image-specific, RF-based supervised classification is a commonly-used, non-parametric machine learning algorithm relatively insensitive to random noise and overfitting (Breiman, 2001). This supervised classification was performed in five steps. First, to generate pan-sharpened multispectral bands at a 0.5-m resolution of WorldView-2 imagery for classification, we fused the eight multispectral bands with the panchromatic band of each image with the widely-used Gram-Schmidt transformation (Aiazz et al., 2009). Second, to obtain representative training samples for the three types of endmembers, we

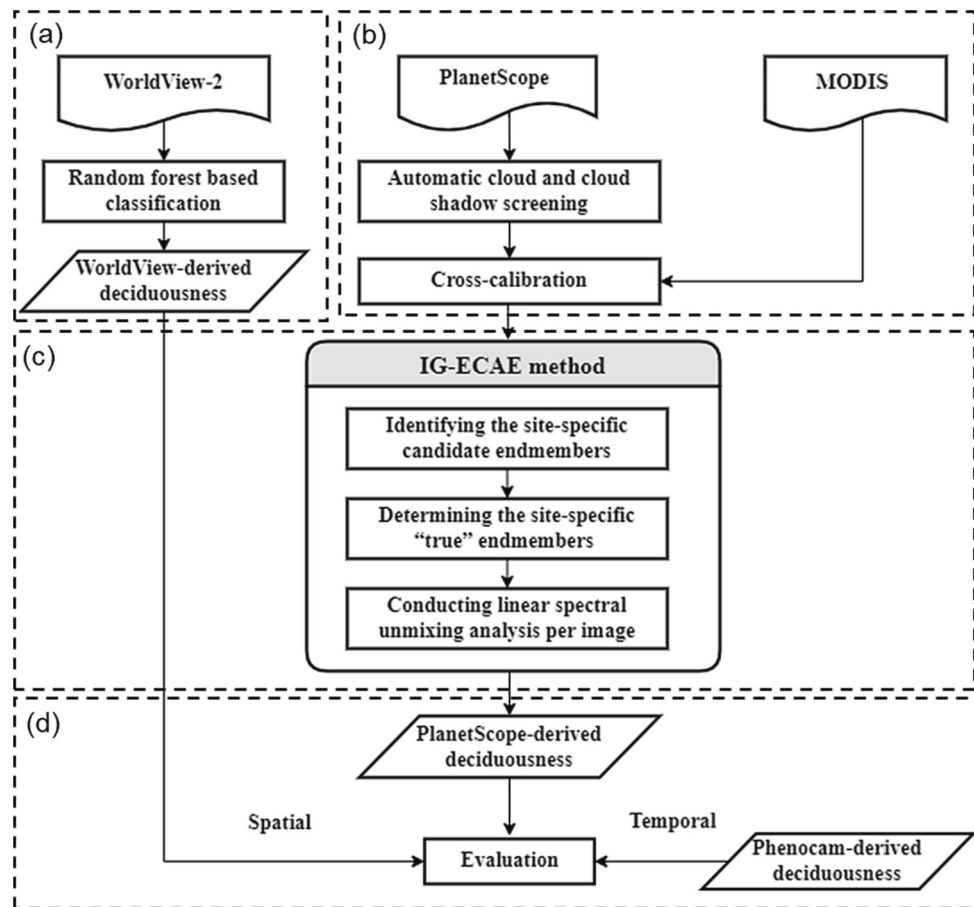


**Fig. 2.** Flowchart of the method. (a) Estimating WorldView-2-derived deciduousness using a random forest (RF) based classification; (b) pre-processing PlanetScope data; (c) estimating deciduousness from PlanetScope data using index-guided, ecologically constrained autoencoder (IG-ECAE) method; (d) evaluating the PlanetScope-derived deciduousness at two dimensions (spatial and temporal), against WorldView-2- and phenocam-derived deciduousness, respectively.

visually labelled leafy canopies (covered by all leaves), leafless canopies (covered by bare and illuminated branches), and deeply shaded areas, all of which were randomly and evenly distributed within each WorldView-2 image. We obtained about 260,000 pixels from each image labelled as the three classes. Third, for each image, we trained and evaluated the supervised classification model with a commonly-used five-fold cross-validation method (Kohavi, 1995). This method randomly splits all labelled pixels into five groups of equal size, with any of the four groups allocated to model training and the remaining group allocated to model testing. The process is iterated until every possible combination of groups has been used for evaluation. The mean overall accuracy (OA) of all these iterations was calculated for the final model performance evaluation. In addition to OA, two additional metrics, producer's accuracy (PA) and user's accuracy (UA) of each class were also calculated across the testing set from a confusion matrix (Congalton, 1991). Fourth, we applied the trained RF model to the entire image and generated a classification map. Fifth, with the derived classification map, we calculated the deciduousness metric at the patch level (i.e., a 90 m × 90 m square area), following an assumption that the shade effect happens equally to the leafy and leafless canopies (Souza et al., 2003, 2005). Based on this assumption, we removed the shade abundance of each patch and re-assigned the shade abundance to the other two classes within the patch, leafy and leafless canopies, resulting in their abundance contribution to a patch sums to 1.0.

### 3.2. Pre-processing PlanetScope data

To minimize artifacts due to cloud/cloud shadow contamination, BRDF effect, and inconsistent cross-sensor radiometric calibration existing in PlanetScope data (Wang et al., 2021; Wang et al., 2020), we adopted a two-step pre-processing approach. First, to minimize the artifacts from clouds/cloud shadows, we applied an automatic cloud and shadow screening approach, which has been demonstrated to be effective and scalable across large tropical landscapes (Wang et al., 2021), to PlanetScope time series for each site. Second, to address the BRDF effect and cross-sensor radiometric inconsistency, we calibrated each PlanetScope image to the gap-filled BRDF-adjusted MODIS surface reflectance of the same day, using the band-specific histogram matching approach following Wang et al. (2020). This calibration generates consistent surface reflectance at both MODIS and PlanetScope pixel scales and has been rigorously evaluated in tropical (Wang et al., 2020) and temperate (Wu et al., 2021) forests.

### 3.3. Estimating the deciduousness metric from PlanetScope data

Given that tropical forest upper canopies are very dense and commonly composed of green leaves, bare and illuminated branches, and shadows caused by tall crowns and deep, narrow gaps, we assumed that there are three key endmembers mixed within each pixel: leafy canopies, leafless canopies, and shade. To estimate the deciduousness metric for each PlanetScope image pixel, we developed an index-guided, ecologically constrained autoencoder model (IG-ECAE) that integrates spectral index-based endmember extraction and a deep learning-based autoencoder model with additional ecological constraints. It is noted that a quite different machine learning model was used for PlanetScope (i.e., unsupervised, automatic) compared with that for WorldView-2 (i.e., supervised, image-specific) because it is impossible to create the manual labels for all PlanetScope images, which is quite labor intensive and not scalable. There are three steps in IG-ECAE, illustrated with details as follows.

#### 3.3.1. Step 1—Identifying candidate endmembers based on spectral indices characteristics

We used an ensemble of five spectral indices (Table 2), including four VIs (i.e., NDVI (Rouse et al., 1974), EVI (Huete et al., 2002), green leaf index (GLI; Johnson et al., 2001), and green red difference index (GRDI;

**Table 2**

Remotely sensed spectral indices used in this study, their equations, and references.

Spectral index	Equation	References
Normalized difference vegetation index (NDVI)	$\frac{NIR - Red}{NIR + Red}$	Rouse et al., 1974
Enhanced vegetation index (EVI)	$2.5 \times \frac{NIR - Red}{(NIR + 6 \times Red - 7.5 \times Blue) + 1}$	Huete et al., 2002
Green leaf index (GLI)	$\frac{2 \times Green - Red - Blue}{2 \times Green + Red + Blue}$	Johnson et al., 2001
Green red difference index (GRDI)	$\frac{Green - Red}{Green + Red}$	Perez et al., 2000
Shadow index (SI)	$\sqrt[3]{(1 - Blue)(1 - Green)(1 - Red)}$	Mon et al., 2012

Blue, Green, Red, and NIR are the reflectances of a PlanetScope pixel at blue, green, red, and NIR bands, respectively.

Perez et al., 2000)) and a shadow index (SI; Mon et al., 2012), to help screen candidate endmembers of leafy canopies, leafless canopies, and shadows from PlanetScope images. The four VIs were used because they are sensitive to leaf chlorophyll content and canopy leaf area, and they have been used to differentiate leafy and leafless canopies (Bhandari et al., 2020; Gitelson et al., 2002; Motohka et al., 2010; Wu et al., 2018). Meanwhile, SI is commonly used for shadow detection in forest areas based on the assumption that shaded areas have lower reflectance in the three visible bands (blue, green, and red) than those illuminated branches and leafy pixels (Sun et al., 2016).

More specifically, for PlanetScope data of each site, we first generated images of all spectral indices, and then identified the candidate endmembers of upper leafy canopy using the intersection of pixels in the top 5% of the four greenness indices: NDVI, EVI, GLI, and GRDI. The candidate endmembers of leafless canopy were identified using the intersection of pixels in the bottom 5% of NDVI, EVI, GLI, and GRDI. The candidate endmembers of shade were identified using the intersection of pixels in the top 5% of SI and in the lowest 5% of NIR. In order to test the impacts of different thresholds of VIs on the final deciduousness estimation of IG-ECAE, we did a sensitivity test on these thresholds using 3%, 5%, and 10%, respectively. We found negligible effects on the final derived deciduousness metric (Fig. S2).

#### 3.3.2. Step 2—Determining the “true” endmembers with an ecologically constrained autoencoder model

With the above-derived candidate endmembers, we then developed an ecologically constrained deep learning-based autoencoder model to refine the endmembers further. An autoencoder model is a feedforward, unsupervised neural network, and consists of two components: an encoder and a decoder, with the former mapping the input data into a low-dimensional representation and the latter mapping this representation back into a reconstruction of the input data (Hinton et al., 2006). This model was used here for two reasons. First, it has been widely used for endmember extraction and abundance mapping with ‘multispectral PlanetScope images’ as ‘the input data’, ‘an abundance map’ as ‘the low-dimensional representation’, and ‘endmember spectra’ as ‘a weight matrix’ for data reconstruction. Second, compared with traditional endmember extraction methods (e.g. vertex component analysis and pixel purity index), the structure of a deep learning-based autoencoder is nonlinear and has higher flexibility (Su et al., 2019), with demonstrated improvements in both accuracy and computational efficiency for endmember extraction and abundance mapping (Min et al., 2021; Qu and Qi, 2019). For details regarding the autoencoder model used in this study refer to Ozkan et al. (2019).

The autoencoder models rely on some simple optimization disciplines (i.e. loss functions) that can generate outcomes with unreasonable

endmembers (e.g. leafless canopies with higher NIR reflectance than leafy canopies). To reduce these problems and improve the accuracy of automatic endmember extractions, we also included prior ecological knowledge of the spectral differences among endmembers as additional constraints. Such an ecologically constrained autoencoder model includes the following four sub-steps.

Sub-step 1: Initialize the three key parameters in the autoencoder model. The first parameter, the weight matrix, indicates endmember-specific reflectance spectra and was initialized with the mean values of the candidate endmembers derived above for each site (see Section 3.3.1). The other two parameters, batch size and learning rate, were respectively set to 1024 and  $1 \times 10^{-5}$  following Min et al. (2021).

Sub-step 2: Determine the rules to break out the iterations of the autoencoder model. The default rule of an autoencoder model used for improving purification of endmember spectra relies on a loss function of mean square error (MSE) that describes the difference between the input and modeled multispectral image reflectances, based on the assumption that the “true” endmember would result in a minimum MSE (or least reconstruction errors). For each iteration, we calculated the difference of MSE before and after the iteration, and repeated the model iteration until the MSE difference was smaller than a given threshold of  $5 \times 10^{-6}$  (Qu and Qi, 2019). To ensure the three output spectra are biophysically meaningful in IG-ECAE, we included three additional constraints based on field-based observations from Carpintero et al. (2020), de Moura et al. (2017), and Wu et al. (2018), including 1) the output leafy canopy endmember should have the highest NIR reflectance values, followed by the leafless canopy endmember and then the shade endmember; 2) the output leafless canopy endmember should have the highest red band reflectance values, followed by the leafy canopy endmember, and then the shade endmember; 3) the three output “true” endmember spectra should be within the ranges of their respective candidate endmembers as derived above (Section 3.3.1). To assess the effectiveness of these additional ecological constraints, we also cross-compared the modelling results with (IG-ECAE) and without (IG-AE) these constraints.

Sub-step 3: Iterate the autoencoder model. A commonly-used gradient descent algorithm—Adam optimizer (Kingma and Ba, 2015)—was used for the subsequent iterative optimization process until all the rules in Sub-step 2 had been met (minimal MSE and the three additional constraints).

Sub-step 4: Derive the final endmember spectra. The optimized and final endmember-specific spectra were derived from the output of Sub-step 3 or the final weight matrix when the last iteration ended.

### 3.3.3. Step 3—Estimating deciduousness using linear spectral unmixing analysis

With the refined endmembers from Section 3.3.2, we then used a linear spectral unmixing model (Eq. 1) to estimate subpixel endmember abundance for each image pixel.

$$x_i = \sum_{k=1}^3 p_{ki} e_k + \epsilon_i, i = 1, \dots, N \quad (1)$$

where  $p_{ki}$  is the abundance of endmember  $k$  in pixel  $i$ ,  $e_k$  is the reflectance spectrum of the  $k$ th endmember,  $\epsilon_i$  is an error term,  $x_i$  is the reflectance spectrum of pixel  $i$ , and  $N$  is the total number of valid pixels in a given PlanetScope image. The abundance values of this model satisfy the constraints:

$$p_{ki} \geq 0 \forall k = 1, \dots, M; \sum_{k=1}^3 p_{ki} = 1. \quad (2)$$

Similar to the deciduousness metric derived from WorldView-2 (Section 3.1), we also followed Souza et al. (2003, 2005) and Wang et al. (2020), and re-assigned the shade fraction of each pixel to the other two endmembers of leafy and leafless canopies. Our sensitivity analysis demonstrates that the reassignment results are better than its correspondence without the reassignment of the shade fraction (Fig. S3). This might be because such reassignment could minimize the sun angle/

environment-induced shade contamination on the extracted deciduousness phenology over the seasons.

### 3.4. Evaluating the accuracy of the PlanetScope-derived deciduousness metric

The PlanetScope-derived deciduousness metric was evaluated at two dimensions (spatial and temporal), against WorldView-2 images ( $n = 9$  sites) and the compiled tower-based phenocam images ( $n = 9$  sites), respectively.

(1) Spatial evaluation: comparison with WorldView-2-derived deciduousness.

We had two objectives for the spatial evaluation: 1) to compare the consistency of spatial variations of PlanetScope-derived classification with those derived from WorldView-2 images, and 2) to examine the relationship between the PlanetScope-derived deciduousness metric aggregated to the patch level and the corresponding metric derived from WorldView-2 images, both within and across forest sites. For the first objective, we generated the classification map from PlanetScope (assigning each pixel by the dominated endmember class) and WorldView-2 of the same/closest date and cross-compared the deciduousness hotspots between the paired maps. For the second objective, we first aggregated the derived classification map to 90 m × 90 m patch sizes to minimize the impact of geometric errors between multi-source remote sensing images (Deng and Wu, 2013). Afterwards, we analysed the linear relationships of patch-level deciduousness between PlanetScope and WorldView-2 both within and across forest sites using the square of correlation coefficient ( $r^2$ ) and root mean square error (RMSE) for accuracy assessment. To assess the effects of patch size on our evaluation, we also performed the same analysis at two other aggregation scales: 30 m × 30 m (similar to the Landsat spatial resolution) and 480 m × 480 m (similar to the MODIS spatial resolution), and found that the results are overall comparable as the assessments performed at the 90 m × 90 m patch size (Fig. S4).

(2) Temporal evaluation: comparison with phenocam-derived deciduousness.

We also assessed the agreement in seasonal deciduousness between PlanetScope and phenocams. For phenocams, we derived ecosystem-scale deciduousness (the fraction of leafless crowns among all crowns in a phenocam view) through time as our benchmark. For PlanetScope, we first derived the deciduousness seasonality corresponding to the field of view of each phenocam site (Burke and Rundquist, 2021; Wu et al., 2016; Yan et al., 2019), we then compared the PlanetScope-derived deciduousness seasonality with the benchmark seasonality derived from phenocams. A linear regression was used for the cross-comparison analysis for each of the 9 sites, and the accuracy was assessed using  $r^2$  and bias that is represented by the difference in maximum deciduousness between PlanetScope and phenocam over the full annual cycle.

(3) Comparison between deciduousness and EVI seasonality respectively derived from PlanetScope.

In the end, we assessed the agreement between the seasonality of deciduousness and EVI respectively derived from PlanetScope. The assessments were performed at two levels: 1) site-specific (for each of the 9 phenocam sites) and 2) across all sites (by pulling all the monthly metrics of deciduousness and EVI for each site covering the full annual cycle and across all 16 sites). The agreement for the former scenario was assessed with the  $r^2$  metric based on a linear regression analysis; the agreement for the latter scenario was assessed with the  $r^2$  metric and a two-segment piecewise regression for a breakpoint analysis.

## 4. Results

### 4.1. Spatial accuracy assessment with WorldView-2 images

For large area spatial evaluations of our PlanetScope results, we used the deciduousness metric derived from WorldView-2 images as the

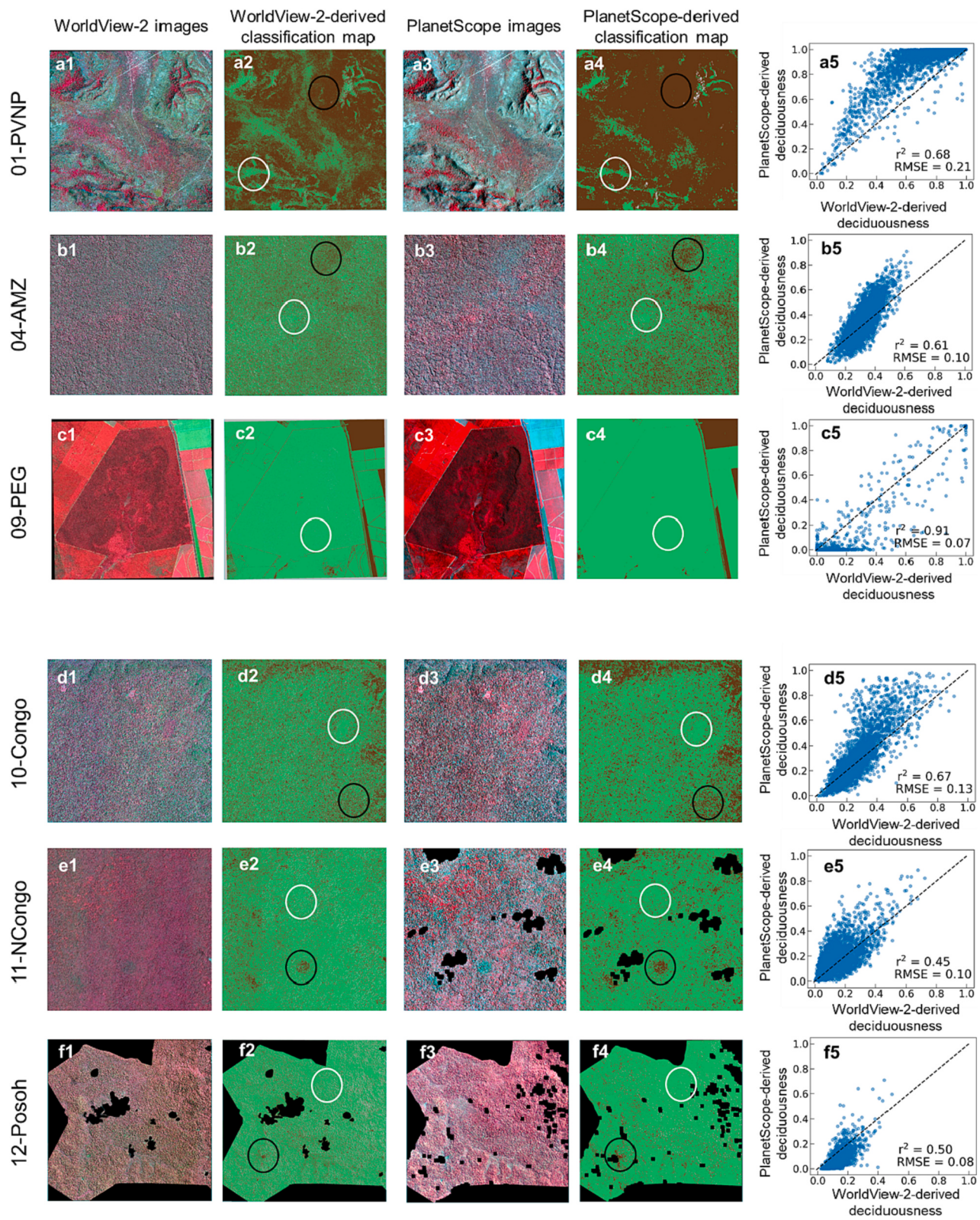


**Fig. 3.** Comparisons of PlanetScope- and WorldView-2-derived classification maps across nine sites having coverage for both sensors. False colour composites (R-G-B = NIR-Red-Green) of WorldView-2 (column a1-i1), PlanetScope images (column a3-i3), and corresponding classification maps derived from image-specific random forest-based classification (column a2-i2) and IG-ECAE (column a4-i4), respectively. The scatter plots of agreement (column a5-i5) compare PlanetScope-derived deciduousness against the corresponding deciduousness derived from WorldView-2 images within 90 m × 90 m patches. The black/white circles in the two classified columns represent major leafless/leafy canopy hotspots. Colour legend for the two classified columns shows leafy canopy pixels in red, leafless canopy pixels in green, and shade pixels in gray. (For interpretation of the references to colour in this figure legend, the reader is referred to the web version of this article.)

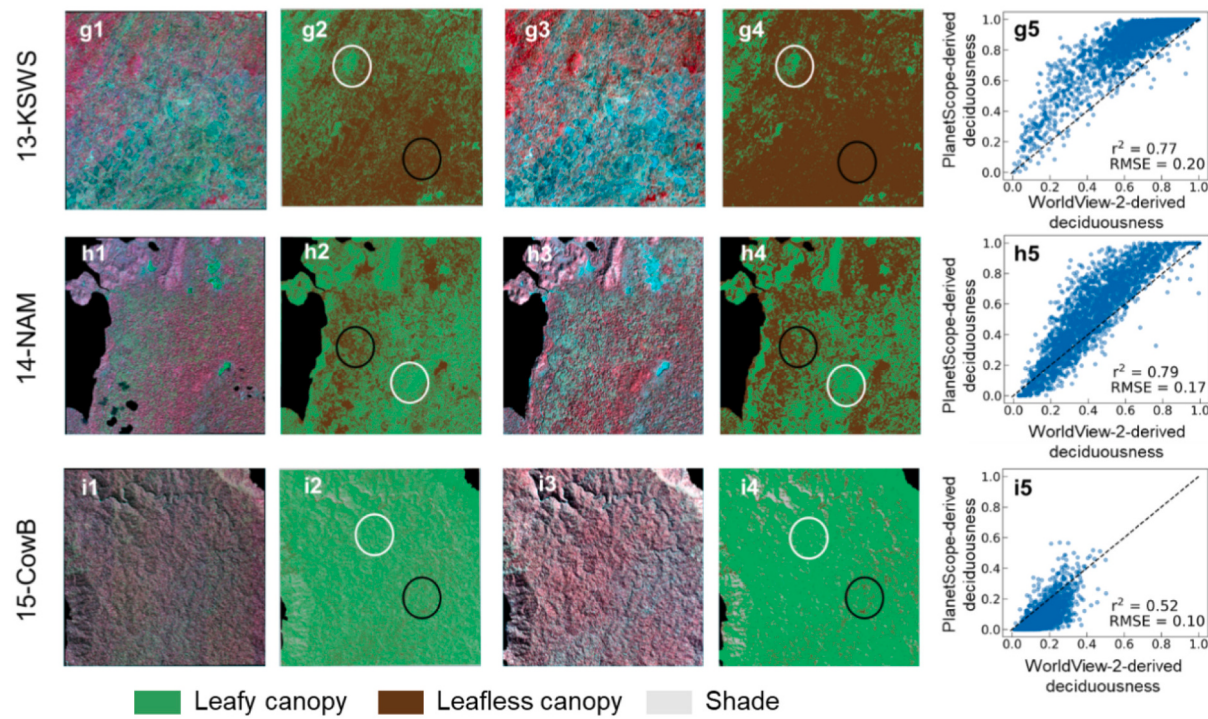


Fig. 3. (continued).

benchmark. As shown in Fig. S5 and Table S2, the image-specific random forest model yielded consistently high accuracies (>95%) for separating leafy canopies, leafless canopies, and shaded areas in the WorldView-2 images, when using OA, PA, and UA as accuracy metrics across all the nine WorldView-2 images, providing a reliable benchmark for evaluating the corresponding metric derived from PlanetScope.

The comparison between PlanetScope and WorldView-2 was analysed on two levels, qualitative and quantitative. Qualitatively, with classification maps generated from both PlanetScope and WorldView-2 (Fig. 3), we observed that both satellites detected large variations in leafless canopy abundance across all 9 tropical forest sites, with 01-

PVNP, 13-KSWS, and 14-NAM having high deciduousness ( $\geq 50\%$ ), followed by 04-AMZ, 10-Congo, and 11-NCongo with moderate deciduousness abundance (16–35%), and 09-PEG, 12-Posoh and 15-CowB with very low deciduousness abundance (<13%). Within each tropical forest site, the leafless canopy abundance displayed considerable spatial heterogeneity across the forest landscapes. Yet, PlanetScope can accurately map the major leafless/leafy canopy hotspots (black/white circles) both within and across tropical forest sites when compared with WorldView-2 (Fig. 3 panel 2 vs. panel 4). There remain some differences between the two satellite sensors, including the spatial extent of each target hotspot and other minor details, likely because of different spatial resolutions

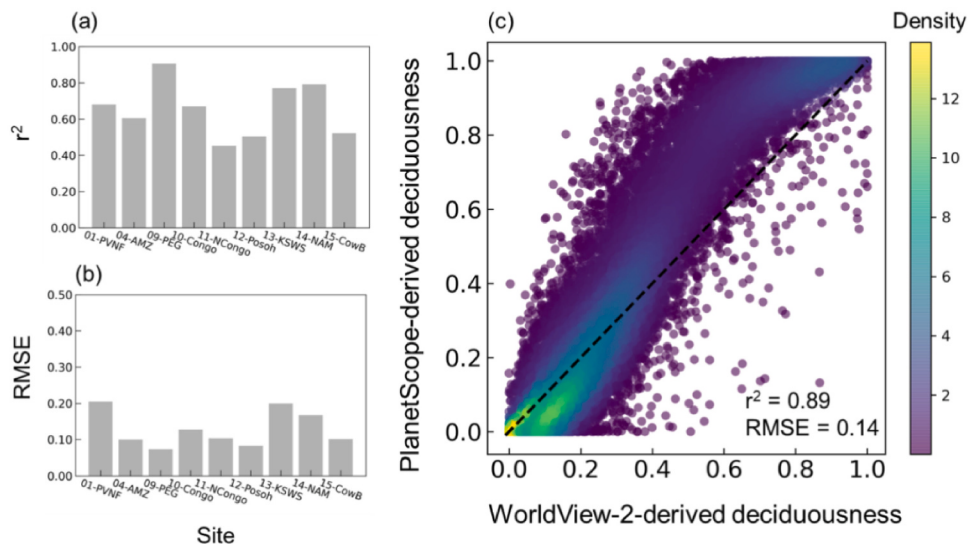


Fig. 4. Evaluation of agreement between the PlanetScope-derived deciduousness within  $90 \text{ m} \times 90 \text{ m}$  patches against corresponding WorldView-2-derived deciduousness across nine sites, including bar charts of site-specific (a)  $r^2$ , (b) RMSE, and (c) scatter plot of agreement for all sites combined. The black dashed line indicates the 1:1 line.

and slight differences in the image acquisition dates associated with these two satellite sensors.

To quantitatively assess the accuracy and scalability of the IG-ECAE method across large environment gradients, we compared the patch-level leafless canopy abundance between PlanetScope and WorldView-2 both within and across all 9 tropical forest sites (Figs. 3 and 4). Our results show that the two measures overall agree well with each other. Within forest sites, we observed  $r^2$  ranging from 0.45 to 0.91 and a RMSE ranging from 0.07 to 0.21 (Fig. 3 panel 5 and Figs. 4a and b). We also observed a much lower  $r^2$  but a quite comparable RMSE ( $r^2 < 0.6$ , RMSE  $\leq 0.14$ ; Figs. 3 e5, f5, i5) at 11-NCongo, 12-Posoh, and 15-CowB sites relative to the other sites, primarily associated with the much narrower range of the deciduousness metric in these sites ( $>90\%$  deciduousness values  $<0.5$ ). However, when pooling the patch level data from all sites, we observed a much tighter relationship between PlanetScope and WorldView-2-derived deciduousness, with  $r^2$  of 0.89 and RMSE of 0.14 (Fig. 4c).

#### 4.2. Temporal accuracy assessment with phenocam images

For temporal-wide evaluations of our PlanetScope results, we used local phenocam images as the benchmark. As shown in Fig. 5, phenocams observed large site-level phenology variability (indicated by the ecosystem-scale deciduousness metric of each site) across all the study sites, with 02-BCI and 09-PEG having strong seasonality, followed by 03-PNM, 05-RJA, 06-ATTO, 07-k67, and 08-Core with moderate seasonality and 15-CowB and 16-RobC with little-to-no seasonality. Still,

PlanetScope-derived deciduousness seasonality correctly captured the leaf phenology patterns as detected by local phenocams, with  $r^2$  ranging from 0.62 to 0.96 across all the sites, except for 15-CowB and 16-RobC, for which we did not estimate  $r^2$  due to the lack of a clear seasonality being displayed by these two sites in their phenocam images. We also observed a relatively lower  $r^2$  ( $r^2 < 0.7$ ; Figs. 5d and e) at 06-ATTO and 07-k67 sites, probably due to a narrow range of the ecosystem-scale deciduousness metric (e.g. 0.0–0.2) across the whole year in these sites. In addition to the seasonal trend, for most study sites, PlanetScope-derived deciduousness metric also tracked the phenocam-derived ecosystem-scale deciduousness metric well in terms of the magnitude, with the magnitude difference between PlanetScope and phenocams ranging from 0.01 to 0.07 across all sites (absolute value of bias; Fig. 5). Notably, the 07-k67 site had a slightly larger magnitude difference between PlanetScope- and phenocam-derived deciduousness. This relatively large difference might be in part attributed to the mismatch in temporal coverage of PlanetScope and phenocam measurements (PlanetScope from 2018 to 2020 and Phenocam data from 2010 to 2011) at this site. Collectively, these results demonstrate that the PlanetScope-derived deciduousness metric can reliably capture tropical forest leaf phenology both in terms of the seasonal trend and the magnitude of seasonal fluctuations.

#### 4.3. Comparison between deciduousness and EVI derived from PlanetScope

To explore the potential advantages and disadvantages of the

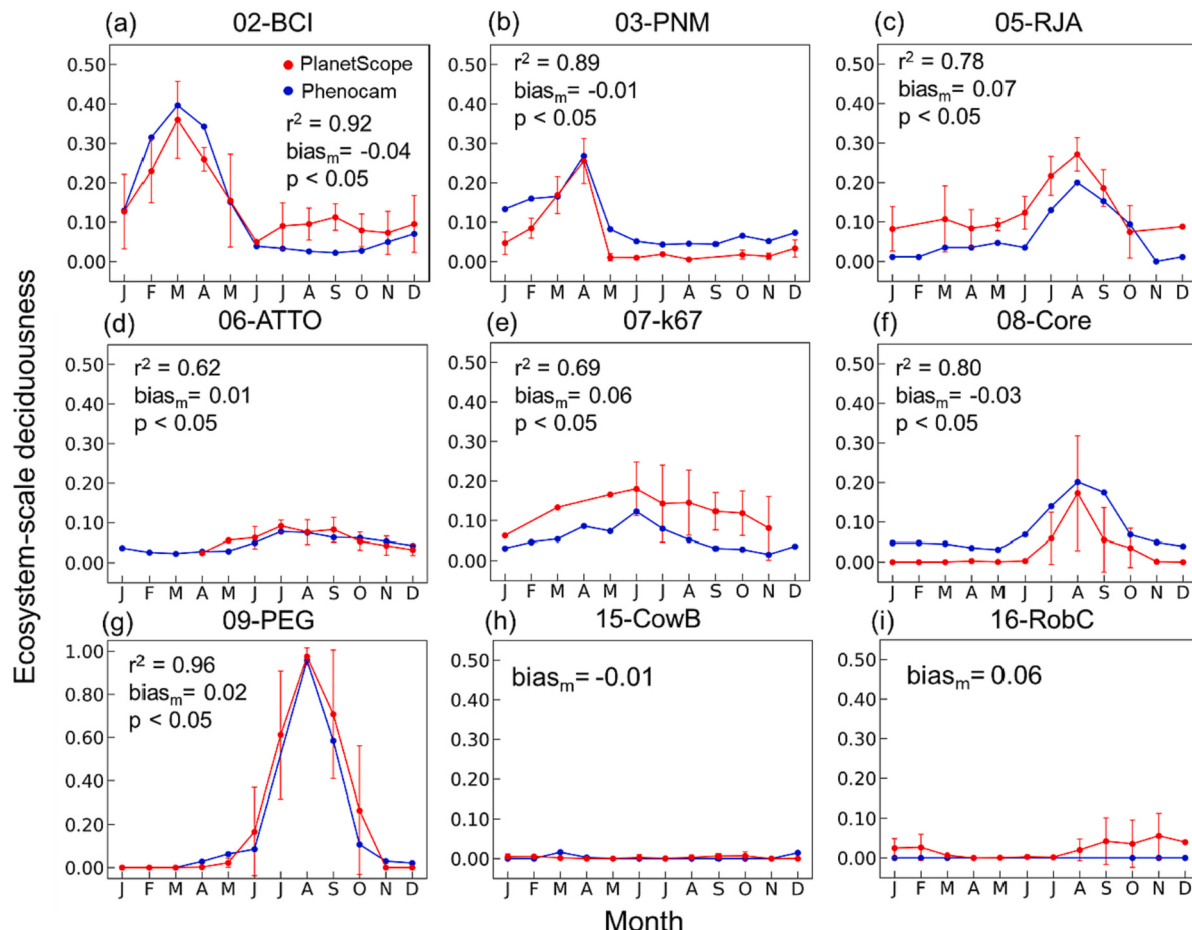


**Fig. 5.** Evaluation of agreement for seasonality of ecosystem-scale deciduousness derived from PlanetScope (red lines) against the fraction of leafless crowns visually assessed in phenocam images (blue lines) across nine phenocam sites. Error bars indicate one standard deviation. (For interpretation of the references to colour in this figure legend, the reader is referred to the web version of this article.)

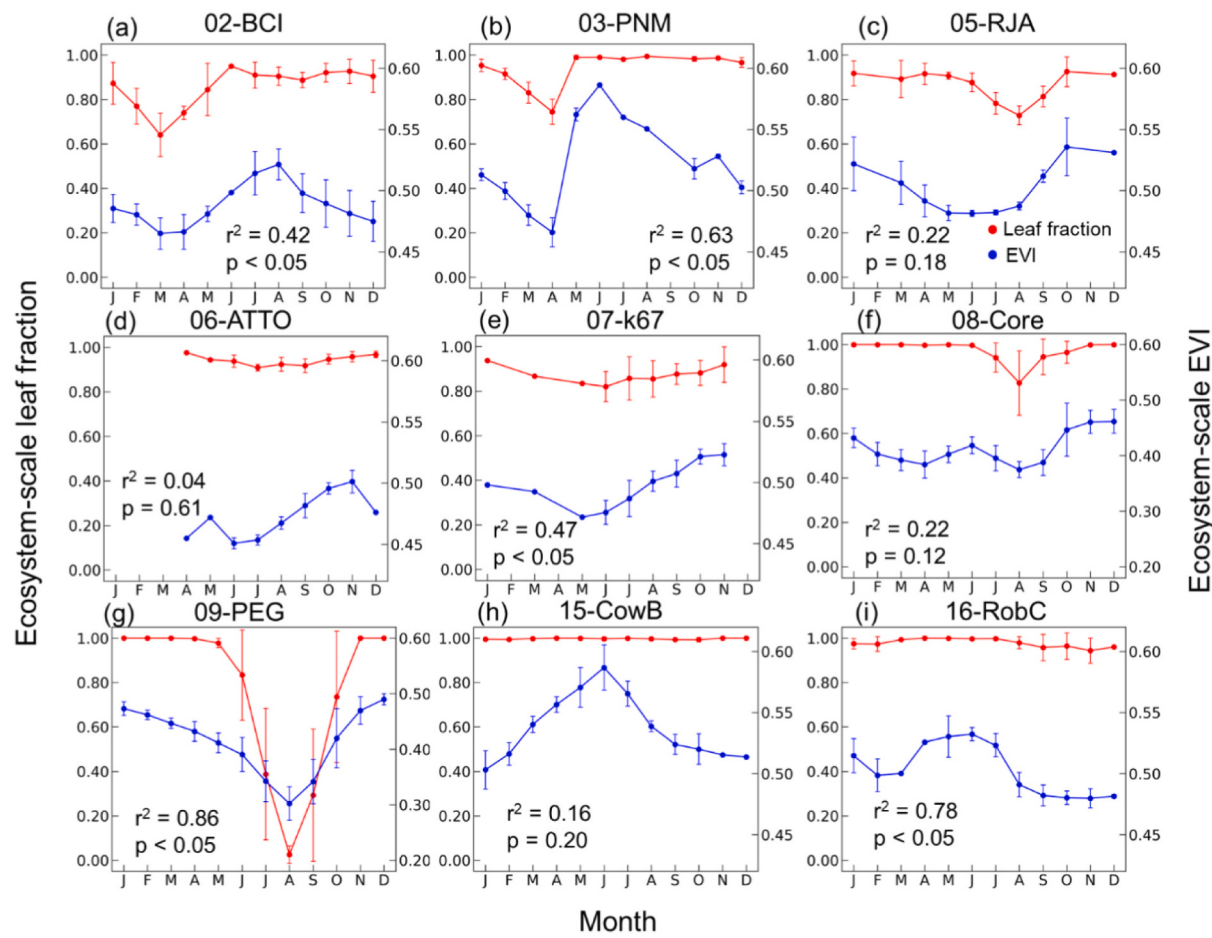


**Fig. 6.** Ecosystem-scale seasonality of leaf fraction (1-deciduousness; the red lines) and EVI (blue lines), both derived exclusively from PlanetScope, across nine phenocam sites. Error bars indicate one standard deviation. (For interpretation of the references to colour in this figure legend, the reader is referred to the web version of this article.)

proposed deciduousness metric, we further compared it to EVI derived from PlanetScope. As shown in Fig. 6, for most of our study sites, EVI and deciduousness overall displayed similar within-site seasonality, with a  $r^2$  ranging from 0.04 to 0.86 across all the study sites. However, there remain two major differences between the two metrics. First, for most sites, in the middle to late growing seasons when the deciduousness metric remains constant, EVI already declines. This is likely associated with the leaf aging processes (e.g. Lopes et al., 2016; Wu et al., 2018; Song et al., 2022). Particularly, for certain sites of evergreen forests (15-CowB and 16-RobC), EVI displayed clear seasonality, in contrast with almost no seasonality in deciduousness or leaf fraction metric (=1-deciduousness) (Fig. 6h and i) and also with the previous phenocam analyses. Second, for a given deciduousness value (e.g. 0.2 in deciduousness and 0.8 in leaf fraction as shown in Fig. 6), there could be large variations in EVI both within each site across seasons and different sites. Because of these two issues, when pooling all the ecosystem scale PlanetScope-derived paired measurements of EVI and deciduousness across the annual cycles and all sites, we observed an overall weak and complex relationship between these two metrics ( $r^2 = 0.43$ ,  $p < 0.05$ ; Fig. 7). In other words, there is a two-segment piecewise linear relationship between deciduousness and EVI: when the deciduousness metric is  $>0.25$ , we found a tight, linear relationship between the two metrics; when the deciduousness metric is  $<0.25$ , the relationship became more scattered with a large range of EVI variability corresponding to a given deciduousness value.

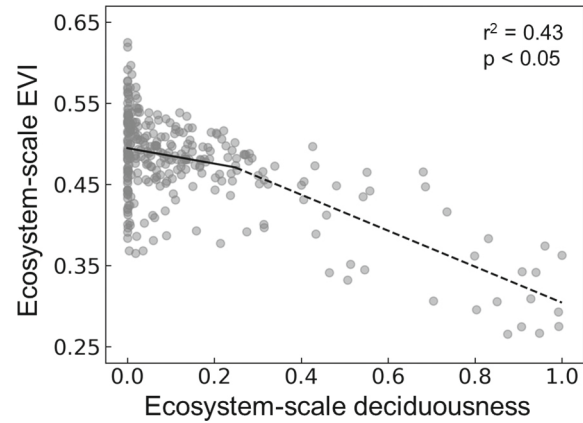


**Fig. 7.** A scatter plot comparing monthly mean deciduousness against EVI, at the ecosystem scale across full annual cycles for all sixteen sites shown in Fig. 1. Both metrics are derived from PlanetScope data. The black line shows a two-segment piecewise linear regression with a breakpoint at ecosystem-scale deciduousness of 0.25.

## 5. Discussion

Cost-effective and scalable monitoring of tropical forest leaf phenology from fine- to ecosystem-scale over large tropical areas is

critical to tropical ecology studies ranging from biogeochemical cycles and modelling to forest response to climate change, but remains challenging to characterize using satellites. Here we developed and evaluated an index-guided, ecologically constrained autoencoder (IG-ECAE) method for cross-scale leaf phenology monitoring in tropical forests using high-resolution PlanetScope data. Our results demonstrated that with the IG-ECAE method PlanetScope-derived deciduousness accurately captured spatial ( $r^2 = 0.89$ ; Fig. 4) and seasonal ( $r^2 = 0.62$  to  $0.96$ ; Fig. 5) variability in the upper forest canopy leafless phenophases, with demonstrated scalability across all tropical sites examined.

### 5.1. Methodological advancements of IG-ECAE

The major advance of IG-ECAE is using additional ecological constraints embedded in the autoencoder deep learning method, which improves the accuracy of endmember purifying and subsequent deciduousness characterization across both sites and seasons. Although conventional autoencoder deep learning methods can also be applied for abundance mapping and have been examined in hyperspectral images previously (Dopido et al., 2012; Han et al., 2021; Min et al., 2021; Xu et al., 2019), most of these methods were evaluated with limited data sets at local sites and their scalability over large spatial areas was rarely tested. Our comparison of model accuracies between spectral index-guided autoencoders with and without additional ecological constraints demonstrated that the overall accuracy in mapping forest deciduousness is much improved ( $r^2$  increased from 0.48 to 0.89; Figs. 4 and S6) when the proposed ecological constraints were used, suggesting the effectiveness and significance of including ecological constraints to improve endmember purifying and subsequent characterization of deciduousness using PlanetScope images. The underlying reasons could be 1) satellite-derived VIs can be effective for screening the candidate endmembers as suggested by many previous studies (Deng and Wu, 2013; Sun et al., 2016); and 2) including three additional ecological constraints can not only return ‘mathematically optimal’ endmembers with comparable least MSE as conventional autoencoder methods (Palsson et al., 2021; Su et al., 2019) but also being ‘biophysically meaningful’ to satisfy spectral characteristic differences among key endmembers. To the best of our knowledge, the ecologically constrained autoencoder deep learning method has not previously been proposed nor evaluated for deciduousness mapping in tropical forests. In the broader Earth system science fields, a growing number of studies have suggested that integrating domain knowledge of physical and biological sciences with deep learning would help lead to better information extraction from big Earth system science data (Read et al., 2019; Ryu et al., 2019). Our work, together with these recent works, suggest that knowledge-constrained-/–guided deep learning methods can be a promising step forward in making better use of big Earth observation data in general (Rasp et al., 2018; Reichstein et al., 2019). The similar approaches as presented in this study can likely be adapted to other pertinent domains of interest, such as image segmentation, classification, and reconstruction.

In addition to testing the effectiveness of including ecological constraints for forest deciduousness characterization, we also explored the optimal way to include these ecological constraints in our proposed IG-ECAE method. Since IG-ECAE used spectral indices plus ecological constraints to guide the autoencoder method for endmember purifying, the major issue is how to integrate these steps (or whether such integrations should be conducted on an image or a site basis). To address this issue, we cross-compared the two scenarios (image- vs. site-specific) (Figs. S7 vs. 4), and found that the site-specific scenario significantly and consistently improved model performance across 9 WorldView-2 images, with an average improvement of overall accuracy of  $r^2$  from 0.36 to 0.89. This is likely because some critical endmember (e.g. fully leafy or fully leafless canopies) are less abundant in certain seasons (e.g. early/late dry season plus wet season with least leafless canopies endmember and middle dry season for very dry sites with least leafy

canopies endmember), and thus the image-specific IG-ECAE could work well for some cases but not always. By contrast, using the seasonal images of a site would provide sufficient pure pixels for each endmember that can further minimize the uncertainty associated with endmember extraction, especially in some time windows when certain endmembers become extremely rare or a certain image is seriously contaminated by (thin) clouds.

Relative to other deep learning-based methods (Host et al., 2020; Laurin et al., 2016) that often rely on large sets of training samples for abundance mapping, our proposed IG-ECAE method is advantageous for being fully automatic, as no prior training data sets are needed. Meanwhile, our evaluations across 16 representative forest sites from 5 continents and spanning a large gradient of mean annual rainfall (1470–2819 mm) also showed highly consistent agreements between PlanetScope-derived deciduousness and the fully independent benchmark (Figs. 4 and 5), demonstrating the great effectiveness and scalability of IG-ECAE for cross-scale tropical phenology monitoring. Such successful cross-evaluations further suggest that our IG-ECAE method could be readily adopted and integrated into monitoring frameworks to cover large geographical areas in the tropics for phenology monitoring.

Notably, spatial resolution could be another issue affecting the accuracy of endmember extractions, as it could affect the accuracy of endmember extraction and thus influence abundance estimation. As shown by many field- and drone-based studies (Blanchard et al., 2016; Park et al., 2019), most upper canopy tree crowns in tropical forests have a crown diameter smaller than 10 m, as such, the conventional satellite remote sensing with coarser resolutions (e.g. Sentinel-2 of 10-m, Landsat of 30-m, and MODIS of 500-m) might not be sufficient to resolve individual tree-crown scale monitoring, resulting in potentially large uncertainty in the endmember extractions of pure leafy and leafless tree-crown statuses. In addition, high temporal resolution is needed to resolve the high temporal variability of tropical leaf phenology. Relative to Landsat and Sentinel-2, PlanetScope satellites, with both higher spatial and temporal resolutions (3-m resolution and near-daily revisit interval) and a global-scale coverage, provide unique data for monitoring the phenology variability across various scales with reduced uncertainty (Cheng et al., 2020; Gao and Zhang, 2021; Moon et al., 2021; Torgbor et al., 2022). The success of integrating IG-ECAE with PlanetScope satellites for tropical forest deciduousness phenology monitoring further suggests that the 3-m resolution could be sufficiently accurate for endmember extraction as expected. With this as a starting point together with the fact PlanetScope data sourcing from the commercial company (with an image cost around US\$1.8/km<sup>2</sup>; assessed from <https://apollomapping.com/planetscope-satellite-imagery>), it would be an essential next step to explore the critical spatial resolution limit of using IC-ECAE for tropical phenology monitoring, by which we would understand whether a similar approach can be extended to Sentinel-2, Landsat, and MODIS satellites with much smaller computational costs and the data on their own being free of charge.

### 5.2. Cross-scale phenology monitoring and opportunities to advance tropical plant ecology studies

With demonstrated effectiveness and scalability as above, our IG-ECAE method when being used with the global coverage of PlanetScope satellite data could provide rich datasets to advance tropical phenology studies, ranging from tracking patterns to understanding drivers. Particularly, relative to the existing phenology products relying on EVI or other VIs (Ganguly et al., 2010; Zhang et al., 2018), PlanetScope-derived deciduousness phenology is advantageous with a clearer biophysical meaning and finer spatial resolution (Figs. 3, 6, and 7). In contrast, commonly used VIs (such as EVI shown in Figs. 6 and 7) are often affected by multiple biophysical and biochemical processes, and the relationships between VIs and key biophysical variables may also vary considerably across sites and seasons associated with the variability in leaf and canopy spectral properties (Brando et al., 2010;

Lopes et al., 2016; Song et al., 2022; Wagner et al., 2017; Wu et al., 2018). PlanetScope-derived deciduousness metric has a clear biophysical meaning showing a tight relationship with leaf quantity. In contrast, PlanetScope-derived EVI is subjected to both leaf quantity and leaf age effect (Wu et al., 2018; Song et al., 2022). The seasonal differences between the deciduousness and EVI metrics thus suggest the possibility of combining these two metrics for monitoring both quantity and quality aspects of tropical phenology, but future attempts with intensive field data remain needed to fully elucidate this potential. Moreover, PlanetScope-derived deciduousness metric would also provide an opportunity to explore the patterns of tropical phenology diversity across landscapes and the drivers of deciduousness phenology diversity both within and across forest landscapes, which remains a critical question in the tropical ecology field (Alberton et al., 2019; Restrepo-Coupe et al., 2017; Wu et al., 2016).

Our method, together with PlanetScope data, will also provide novel opportunities for exploring the role of tropical phenology, particularly the diversity of deciduousness phenology in regulating tropical forest ecosystem metabolism. Tropical forests are globally important as they can uptake more carbon through plant photosynthesis than any other terrestrial biomes (Beer et al., 2010; Mitchard, 2018; Saatchi et al., 2011). Leaf phenology, particularly the diversity of leaf phenology strategies in terms of spatial heterogeneity in leaf on/off status, and associated leaf age demography (Albert et al., 2018; Reich et al., 2004; Wu et al., 2016), has been attributed as major biotic regulators of the seasonality in key ecosystem metabolism, e.g. photosynthesis (Dettlo and Pacala, 2022; Wu et al., 2016; Xia et al., 2015), net ecosystem exchange (Girardin et al., 2016; Hayek et al., 2018), and isoprene emission (Alves et al., 2018; Wei et al., 2018) in the tropics. However, it remains a major source of uncertainty for interpreting ecosystem-scale metabolism seasonality and improving terrestrial biosphere modelling of tropical forest response to climate change (Albert et al., 2019; Restrepo-Coupe et al., 2017). With PlanetScope-derived deciduousness phenology, together with the increasing availability of eddy covariance data across the tropics (Pastorello et al., 2020) and pan-tropical measurements of satellite-based solar-induced fluorescence (e.g. large-scale photosynthesis proxy; Frankenberg et al. (2011); Magney et al. (2019); Yang et al. (2015)) and NIRv (another demonstrated proxy for ecosystem photosynthesis; Badgley et al. (2017)), it could offer great potential to improve the understanding and modelling of seasonal and spatial variation in phenology-photosynthesis metabolism associations in the tropics.

### 5.3. Caveats and future directions

Our study also identifies at least three next steps that need to be considered for future advances. First, we observed that although the seasonal trend in ecosystem-scale deciduousness derived from PlanetScope is well correlated with that from phenocams across the entire annual cycle (Fig. 5), there remain certain magnitude differences between these two independent data sources. This is likely because of the mismatch of spatial extents and temporal periods between these different data sources (Table 1). Also, flowering, brown leaves, and understory materials in tropical trees might affect the deciduousness estimation (Carvalho et al., 2013; Pau et al., 2018; Wu et al., 2021). However, due to the limited spatial and spectral resolution of PlanetScope data, it would be challenging to expand the current three end-members to four or more endmembers (e.g. fully green leaves, fully brown leaves, fully leafless, fully flowers, and fully shaded). Since proximate remote sensing observations of the same years may provide more consistent comparisons with sufficient spatial coverage (Lopes et al., 2016; Meng et al., 2018; Park et al., 2019) and the integration with deep learning can also help quantify such impacts on deciduousness estimation (Chen et al., 2019; Dixon et al., 2021), we thus recommend integrating PlanetScope data with drone surveys and LiDAR data (Meng et al., 2018; Wu et al., 2021) for further comprehensive accuracy assessments in the future attempts. Second, although the IG-ECAE method

was tested for 16 well-preserved forest sites across all five continents in the tropics, the shade reassignment assumption used in this study may introduce some uncertainties when extending our method to those non-closed forests with large-sized canopy gaps, especially in disturbed and fragmented forest areas or heterogeneous landscapes mixed with different land cover types (e.g. croplands, bare soil, or wetlands). To investigate the impacts of canopy gaps, we now included a simulated mask that helps screen out the canopy gaps (those image pixels with a dominated fraction of shaded areas across the whole annual cycle). Our results (Fig. S8) suggest that canopy gaps would have a very limited impact on deciduousness estimation using IG-ECAE, especially in our preserved forest sites; more comprehensive tests in disturbed forests remain needed but this is beyond the scope of this paper. In the meantime, to address this issue, for broader geographical areas, we recommend integrating high-resolution land cover maps (Sulla-Menashe et al., 2019; Zhang et al., 2021) to best aid in masking out those non-forest or fragmented areas. Third, the massive data volumes and high expenses for the high-resolution, commercial PlanetScope satellite data might also hinder the extension of our method to the pan-tropics. Therefore, we recommend using machine learning-based methods to upscale the site-based deciduousness metric derived from PlanetScope to other freely available satellites, such as Landsat or Sentinel-2, which would help map the deciduousness variability across the pan-tropics.

## 6. Conclusions

We have developed and evaluated an index-guided, ecologically constrained autoencoder method, IG-ECAE, for cross-scale leaf phenology monitoring in tropical forests using high-resolution PlanetScope data. This method includes three steps, with step 1 identifying the candidate endmembers with the help of satellite-derived spectral indices, step 2 refining and purifying the endmembers with an autoencoder deep learning model subject to ecological constraints, and step 3 estimating the endmember abundances per pixel with linear spectral unmixing analysis. The method enables automatic characterization of tropical leaf phenology providing a deciduousness metric with clear biophysical meaning. The method has been rigorously evaluated with benchmarks covering both spatial (using WorldView-2 data) and seasonal (using phenocams) dimensions across 16 contrasting sites in the tropics. Across these study sites, IG-ECAE obtains consistently high accuracy with reference to WorldView-2 ( $r^2 = 0.89$ ) and phenocam images ( $r^2 = 0.62$  to  $0.96$ ). With such high accuracy across both space and seasons, we expect that IG-ECAE can become an effective and scalable method for use in analysing PlanetScope data for monitoring tropical phenology. This approach will be important for advancing our understanding of patterns and drivers of tropical leaf phenology diversity as well as in probing the seasonality and variability in tropical forest metabolism across scales.

## Author contributions

Jin Wu, Jing Wang, and Guangqin Song conceived the project idea. Jing Wang and Guangqin Song performed the data analysis, with the critical machine learning support from Michael Ng. Michael Liddell, Patricia Morellato, Bruna Alberton, Matteo Dettlo, and Bruce Nelson shared the phenocam data for evaluation. Michael Liddell, Patricia Morellato, Calvin Lee, Deidi Yang, Bruna Alberton, Matteo Dettlo, Xuanlong Ma, Yingyi Zhao, Henry C.H. Yeung, Hongsheng Zhang, Michael Ng, Bruce Nelson, and Alfredo Huete participated in the result interpretation and rigorousness evaluation of the method. Jing Wang, Guangqin Song, and Jin Wu drafted the manuscript, and all authors contribute to the manuscript editing and revision.

## Declaration of Competing Interest

The authors declare that they have no known competing financial

interests or personal relationships that could have appeared to influence the work reported in this paper.

## Data availability

Data will be made available on request.

## Acknowledgements

This work was supported by National Natural Science Foundation of China (#31922090), Hong Kong Research Grant Council General Research Fund (#17316622) and the São Paulo Research Foundation – FAPESP (grants FAPESP – Microsoft Research Institute #2013/50155-0, #2019/11835-2, 2019/16191-6). J. Wang was in part supported by Shenzhen Science and Technology Program (Grant No. 20220816162849005) and the Division of Ecology and Biodiversity PDF research award. CKFL was in part supported by HKU seed fund for basic research (#202011159154) and the HKU 45th round PDF scheme. DY was supported by the United States Department of Energy contract No. DE-SC0012704 to Brookhaven National Laboratory. BA received PhD fellowships from FAPESP (#2014/00215-0 and #2016/01413-5) and a Post-doctoral fellowship from CAPES Print Program (#88887.512218/2020-00) at UNESP. LPCM receives research productivity fellowships from National Council for Scientific and Technological Development (CNPq grant #428055/2018-4). XM was supported by the National Natural Science Foundation of China (42171305), the Natural Science Foundation of Gansu Province, China (21JR7RA499), the Director Fund of the International Research Center of Big Data for Sustainable Development Goals (CBAS2022DF006), and the Open Fund of Key laboratory of Geographic Information Science (Ministry of Education), East China Normal University. M. Ng was supported in part by Hong Kong Research Grant Council GRF 12300519, 17201020, 17300021, C1013-21GF, C7004-21GF and Jointly by NSFC-RGC N-HKU76921. Phenocam data collection at the Australian sites was supported by the Australian Government's Terrestrial Ecosystem Research Network (TERN, [www.tern.org.au](http://www.tern.org.au)). Phenocam data collection at the Amazon Tall Tower tower was supported by the Brazilian Ministry of Science, Technology and Innovation (MCTI) and the German Federal Ministry of Education and Research (BMBF).

## Appendix A. Supplementary data

Supplementary data to this article can be found online at <https://doi.org/10.1016/j.rse.2022.113429>.

## References

- Adams, J.B., Sabol, D.E., Kapos, V., Almeida, R., Roberts, D.A., Smith, M.O., Gillespie, A.R., 1995. Classification of multispectral images based on fractions of endmembers - application to land-cover change in the Brazilian Amazon. *Remote Sens. Environ.* 52, 137–154.
- Aiazzi, B., Baronti, S., Lotti, F., Selva, M., 2009. A comparison between global and context-adaptive pansharpening of multispectral images. *IEEE Geosci. Remote Sens. Lett.* 6, 302–306.
- Albert, L.P., Restrepo-Coupe, N., Smith, M.N., Wu, J., Chavava-Bryant, C., Prohaska, N., Taylor, T.C., Martins, G.A., Ciais, P., Mao, J.F., Arain, M.A., Li, W., Shi, X.Y., Ricciuto, D.M., Huxman, T.E., McMahon, S.M., Saleska, S.R., 2019. Cryptic phenology in plants: case studies, implications, and recommendations. *Glob. Chang. Biol.* 25, 3591–3608.
- Albert, L.P., Wu, J., Prohaska, N., de Camargo, P.B., Huxman, T.E., Tribuzi, E.S., Ivanov, V.Y., Oliveira, R.S., Garcia, S., Smith, M.N., Oliveira, R.C., Restrepo-Coupe, N., da Silva, R., Stark, S.C., Martins, G.A., Penha, D.V., Saleska, S.R., 2018. Age-dependent leaf physiology and consequences for crown-scale carbon uptake during the dry season in an Amazon evergreen forest. *New Phytol.* 219, 870–884.
- Alberton, B., Almeida, J., Helm, R., Torres, R.D., Menzel, A., Morellato, L.P.C., 2014. Using phenological cameras to track the green up in a cerrado savanna and its on-the-ground validation. *Ecol. Informat.* 19, 62–70.
- Alberton, B., Torres, R.D., Silva, T.S.F., da Rocha, H.R., Moura, M.S.B., Morellato, L.P.C., 2019. Leafing patterns and drivers across seasonally dry tropical communities. *Remote Sens.* 11.
- Alves, E.G., Tota, J., Turnipseed, A., Guenther, A.B., Bustillos, J.O.W.V., Santana, R.A., Cirino, G.G., Tavares, J.V., Lopes, A.P., Nelson, B.W., de Souza, R.A., Gu, D., Stavrakou, T., Adams, D.K., Wu, J., Saleska, S., Manzi, A.O., 2018. Leaf phenology as one important driver of seasonal changes in isoprene emissions in Central Amazonia. *Biogeosciences* 15, 4019–4032.
- Arroyo-Mora, J.P., Sanchez-Azofeifa, G.A., Kalacska, M.E.R., Rivard, B., Calvo-Alvarado, J.C., Janzen, D.H., 2005. Secondary forest detection in a neotropical dry forest landscape using Landsat 7 ETM+ and IKONOS imagery. *Biotropica* 37, 497–507.
- Asner, G.P., Knapp, D.E., Balaji, A., Paez-Acosta, G., 2009. Automated mapping of tropical deforestation and forest degradation: CLASlite. *J. Appl. Remote. Sens.* 3.
- Badgley, G., Field, C.B., Berry, J.A., 2017. Canopy near-infrared reflectance and terrestrial photosynthesis. *Sci. Adv.* 3.
- Beer, C., Reichstein, M., Tomelleri, E., Ciais, P., Jung, M., Carvalhais, N., Rodenbeck, C., Arain, M.A., Baldocchi, D., Bonan, G.B., Bondeau, A., Cescatti, A., Lasslop, G., Lindroth, A., Lomas, M., Luyssaert, S., Margolis, H., Oleson, K.W., Roupsard, O., Veendendaal, E., Viovy, N., Williams, C., Woodward, F.I., Papale, D., 2010. Terrestrial gross carbon dioxide uptake: global distribution and covariation with climate. *Science* 329, 834–838.
- Bhandari, M., Ibrahim, A.M.H., Xue, Q.W., Jung, J.H., Chang, A.J., Rudd, J.C., Maeda, M., Rajan, N., Neely, H., Landivar, J., 2020. Assessing winter wheat foliage disease severity using aerial imagery acquired from small unmanned aerial vehicle (UAV). *Comput. Electron. Agric.* 176.
- Bhattarai, R., Rahimzadeh-Bajgiran, P., Weiskittel, A., Meneghini, A., MacLean, D.A., 2021. Spruce budworm tree host species distribution and abundance mapping using multi-temporal Sentinel-1 and Sentinel-2 satellite imagery. *ISPRS J. Photogramm. Remote Sens.* 172, 28–40.
- Blanc, L., Maury-Lechon, G., Pascal, J.P., 2000. Structure, floristic composition and natural regeneration in the forests of Cat Tien National Park, Vietnam: an analysis of the successional trends. *J. Biogeogr.* 27, 141–157.
- Blanchard, E., Birnbaum, P., Ibanez, T., Bouteux, T., Antin, C., Ploton, P., Vincent, G., Pouteau, R., Vandrot, H., Hequet, V., Barbier, N., Droissart, V., Sonke, B., Texier, N., Kamdem, N.G., Zebaze, D., Libalah, M., Couteron, P., 2016. Contrasted allometries between stem diameter, crown area, and tree height in five tropical biogeographic areas. *Trees-Struct. Funct.* 30, 1953–1968.
- Brando, P.M., Goetz, S.J., Baccini, A., Nepstad, D.C., Beck, P.S.A., Christman, M.C., 2010. Seasonal and interannual variability of climate and vegetation indices across the Amazon. *Proc. Natl. Acad. Sci. U.S.A.* 107, 14685–14690.
- Breiman, L., 2001. Random forests. *Mach. Learn.* 45, 5–32.
- Burke, M.W.V., Rundquist, B.C., 2021. Scaling Phenocam GCC, NDVI, and EVI2 with harmonized Landsat-sentinel using Gaussian processes. *Agric. For. Meteorol.* 300.
- Carpintero, E., Andreu, A., Gomez-Giraldez, P.J., Blazquez, A., Gonzalez-Dugo, M.P., 2020. Remote-sensing-based water balance for monitoring of evapotranspiration and water stress of a Mediterranean Oak-Grass Savanna. *Water* 12.
- Carvalho, S., Schlerf, M., van der Putten, W.H., Skidmore, A.K., 2013. Hyperspectral reflectance of leaves and flowers of an outbreak species discriminates season and successional stage of vegetation. *Int. J. Appl. Earth Obs. Geoinf.* 24, 32–41.
- Chen, B., Jin, Y.F., Brown, P., 2019. An enhanced bloom index for quantifying floral phenology using multi-scale remote sensing observations. *ISPRS J. Photogramm. Remote Sens.* 156, 108–120.
- Cheng, Y., Vrieling, A., Fava, F., Meroni, M., Marshall, M., Gachoki, S., 2020. Phenology of short vegetation cycles in a kenyian rangeland from PlanetScope and Sentinel-2. *Remote Sens. Environ.* 248, 112004 <https://doi.org/10.1016/j.rse.2020.112004>.
- Congalton, R.G., 1991. A review of assessing the accuracy of classifications of remotely sensed data. *Remote Sens. Environ.* 37, 35–46.
- de Camargo, M.G.G., de Carvalho, G.H., Alberton, B.D., Reys, P., Morellato, L.P.C., 2018. Leafing patterns and leaf exchange strategies of a cerrado woody community. *Biotropica* 50, 442–454.
- de Moura, Y.M., Galvao, L.S., Hilker, T., Wu, J., Saleska, S., do Amaral, C.H., Nelson, B.W., Lopes, A.P., Wiedeman, K.K., Prohaska, N., de Oliveira, R.C., Machado, C.B., Aragao, L.E.O.C., 2017. J. Spectral analysis of amazon canopy phenology during the dry season using a tower hyperspectral camera and modis observations. *Isprs J. Photogramm. Remote Sens.* 131, 52–64.
- Deng, C.B., Wu, C.S., 2013. A spatially adaptive spectral mixture analysis for mapping subpixel urban impervious surface distribution. *Remote Sens. Environ.* 133, 62–70.
- Detto, M., Pacala, S.W., 2022. Plant hydraulics, stomatal control, and the response of a tropical forest to water stress over multiple temporal scales. *Glob. Chang. Biol.* 28, 4359–4376.
- Detto, M., Wright, S.J., Calderon, O., Muller-Landau, H.C., 2018. Resource acquisition and reproductive strategies of tropical forest in response to the El Nino-southern oscillation. *Nat. Commun.* 9 <https://doi.org/10.1038/s41467-41018-03306-41469>.
- DigitalGlobe, 2021. DigitalGlobe Core Imagery Products Guide. Accessed. <https://www.geosolutions.cl/documentos/worldview/DigitalGlobe-Core-Imagery-Products-Guide.pdf>.
- Dixon, D.J., Callow, J.N., Duncan, J.M.A., Setterfield, S.A., Pauli, N., 2021. Satellite prediction of forest flowering phenology. *Remote Sens. Environ.* 255.
- Dopido, I., Villa, A., Plaza, A., Gamba, P., 2012. A quantitative and comparative assessment of unmixing-based feature extraction techniques for hyperspectral image classification. *Ieee J. Select.Top. Appl. Earth Observ. Remote Sens.* 5, 421–435.
- Forzieri, G., Miralles, D.G., Ciais, P., Alkama, R., Ryu, Y., Duveiller, G., Zhang, K., Robertson, E., Kautz, M., Martens, B., Jiang, C.Y., Arneth, A., Georgievski, G., Li, W., Ceccherini, G., Anthoni, P., Lawrence, P., Wiltshire, A., Pongratz, J., Piao, S.L., Sitch, S., Goll, D.S., Arora, V.K., Lienert, S., Lombardozzi, D., Kato, E., Nabel, J.E.M.S., Tian, H.Q., Friedlingstein, P., Cescatti, A., 2020. Increased control of vegetation on global terrestrial energy fluxes. *Nat. Clim. Chang.* 10, 356–362.
- Frankenberg, C., Fisher, J.B., Worden, J., Badgley, G., Saatchi, S.S., Lee, J.E., Toon, G.C., Butz, A., Jung, M., Kuze, A., Yokota, T., 2011. New global observations of the

- terrestrial carbon cycle from GOSAT: patterns of plant fluorescence with gross primary productivity. *Geophys. Res. Lett.* 38.
- Ganguly, S., Friedl, M.A., Tan, B., Zhang, X.Y., Verma, M., 2010. Land surface phenology from MODIS: characterization of the collection 5 global land cover dynamics product. *Remote Sens. Environ.* 114, 1805–1816.
- Gao, F., Zhang, X., 2021. Mapping crop phenology in near real-time using satellite remote sensing: challenges and opportunities. *J. Remote Sens.* 2021, 1–14. <https://doi.org/10.34133/2021/8379391>.
- Girardin, C.A.J., Malhi, Y., Doughty, C.E., Metcalfe, D.B., Meir, P., del Aguila-Pasquel, J., Araujo-Murakami, A., da Costa, A.C.L., Silva-Espejo, J.E., Amezquita, F.F., Rowland, L., 2016. Seasonal trends of Amazonian rainforest phenology, net primary productivity, and carbon allocation. *Glob. Biogeochem. Cycles* 30, 700–715.
- Gitelson, A.A., Kaufman, Y.J., Stark, R., Rundquist, D., 2002. Novel algorithms for remote estimation of vegetation fraction. *Remote Sens. Environ.* 80, 76–87.
- Gonçalves, N.B., Lopes, A.P., Dalagnol, R., Wu, J., Pinho, D.M., Nelson, B.W., 2020. Both near-surface and satellite remote sensing confirm drought legacy effect on tropical forest leaf phenology after 2015/2016 ENSO drought. *Remote Sens. Environ.* 237.
- Guan, K.Y., Pan, M., Li, H.B., Wolf, A., Wu, J., Medvigy, D., Caylor, K.K., Sheffield, J., Wood, E.F., Malhi, Y., Liang, M.L., Kimball, J.S., Saleska, S.R., Berry, J., Joiner, J., Lyapustin, A.I., 2015. Photosynthetic seasonality of global tropical forests constrained by hydroclimate. *Nat. Geosci.* 8, 284–289.
- Han, Z., Hong, D.F., Gao, L.R., Zhang, B., Chanussot, J., 2021. Deep half-siamese networks for hyperspectral unmixing. *IEEE Geosci. Remote Sens. Lett.* 18, 1996–2000.
- Hayek, M.N., Longo, M., Wu, J., Smith, M.N., Restrepo-Coupe, N., Tapajos, R., da Silva, R., Fitzjarrald, D.R., Camargo, P.B., Hutyra, L.R., Alves, L.F., Daube, B., Munger, J.W., Wiedemann, K.T., Saleska, S.R., Wofsy, S.C., 2018. Carbon exchange in an Amazon forest: from hours to years. *Biogeosciences* 15, 4833–4848.
- Hinton, G.E., Osindero, S., Teh, Y.W., 2006. A fast learning algorithm for deep belief nets. *Neural Comput.* 18, 1527–1554.
- Host, T.K., Russell, M.B., Windmuller-Campione, M.A., Slesak, R.A., Knight, J.F., 2020. Ash presence and abundance derived from composite Landsat and Sentinel-2 time series and lidar surface models in Minnesota, USA. *Remote Sens.* 12.
- Houborg, R., McCabe, M.F., 2018a. A cubesat enabled spatio-temporal enhancement method (CESTEM) utilizing planet, Landsat and MODIS data. *Remote Sens. Environ.* 209, 211–226.
- Houborg, R., McCabe, M.F., 2018b. Daily retrieval of NDVI and LAI at 3 m resolution via the fusion of CubeSat, Landsat, and MODIS data. *Remote Sens.* 10.
- Huechacona-Ruiz, A.H., Dupuy, J.M., Schwartz, N.B., Powers, J.S., Reyes-Garcia, C., Tun-Dzul, F., Hernandez-Stefanon, J.L., 2020. Mapping tree species deciduousness of tropical dry forests combining reflectance, spectral unmixing, and texture data from high-resolution imagery. *Forests* 11.
- Huete, A., Didan, K., Miura, T., Rodriguez, E.P., Gao, X., Ferreira, L.G., 2002. Overview of the radiometric and biophysical performance of the MODIS vegetation indices. *Remote Sens. Environ.* 83, 195–213.
- Huete, A.R., Didan, K., Shimabukuro, Y.E., Ratana, P., Saleska, S.R., Hutyra, L.R., Yang, W.Z., Nemani, R.R., Myneni, R., 2006. Amazon rainforests green-up with sunlight in dry season. *Geophys. Res. Lett.* 33.
- Huete, A.R., Restrepo-Coupe, N., Ratana, P., Didan, K., Saleska, S.R., Ichii, K., Panuthai, S., Gamo, M., 2008. Multiple site tower flux and remote sensing comparisons of tropical forest dynamics in monsoon Asia. *Agric. For. Meteorol.* 148 (5), 748–760.
- Ifo, S.A., Moutsambite, J.-M., Koubouana, F., Yoka, J., Ndzaï, S.F., Bouetou-Kadilamio, L.N.O., Mampouya, H., Jourdain, C., Bocko, Y., Mantota, A.B., 2016. Tree species diversity, richness, and similarity in intact and degraded forest in the tropical rainforest of the Congo Basin: case of the forest of Likouala in the Republic of Congo. *Int. J. Forestry Res.* 2016.
- Johnson, D.E., Harris, N.R., Louhaichi, M., Casady, G.M., Borman, M.M., 2001. Mapping selected noxious weeds using remote sensing and geographic information systems. *Abstr. Pap. Am. Chem. Soc.* 221, U48.
- Keshava, N., Mustard, J.F., 2002. In: Spectral unmixing. *IEEE Signal Processing Magazine*, 19, pp. 44–57.
- Kingma, D., Ba, J., 2015. Adam: a method for stochastic optimization. In: Proc. Int. Conf. Learn. Represent. (ICLR), pp. 1–15.
- Knight, D.H., 1975. Phytosociological analysis of species-rich tropical Forest on Barro Colorado Island, Panama. *Ecol. Monogr.* 45, 259–284.
- Kochummen, K.M., LaFrankie Jr., J.V., Manokaran, N., 1990. Floristic composition of Pasoh Forest Reserve, a lowland rain forest in Peninsular Malaysia. *J. Trop. For. Sci.* 1–13.
- Kohavi, R., 1995. A study of cross-validation and bootstrap for accuracy estimation and model selection. In: Ijcai, pp. 1137–1145. Montreal, Canada.
- Laurin, G.V., Puletti, N., Hawthorne, W., Liesenberg, V., Corona, P., Papale, D., Chen, Q., Valentini, R., 2016. Discrimination of tropical forest types, dominant species, and mapping of functional guilds by hyperspectral and simulated multispectral Sentinel-2 data. *Remote Sens. Environ.* 176, 163–176.
- Liddell, M., Weigand, N., 2021. Phenocam Images and phenology data from TERN Robson Creek Rainforest SuperSite. Version 1.0.0. Terrestrial Ecosystem Research Network (TERN). (Dataset).
- Lopes, A.P., Nelson, B.W., Wu, J., Graca, P.M.L.D., Tavares, J.V., Prohaska, N., Martins, G.A., Saleska, S.R., 2016. Leaf flush drives dry season green-up of the Central Amazon. *Remote Sens. Environ.* 182, 90–98.
- Ma, X.L., Huete, A., Yu, Q., Coupe, N.R., Davies, K., Broich, M., Ratana, P., Beringer, J., Hutley, L.B., Cleverly, J., Boulaïn, N., Eamus, D., 2013. Spatial patterns and temporal dynamics in savanna vegetation phenology across the north Australian tropical transect. *Remote Sens. Environ.* 139, 97–115.
- Maeda, E.E., Moura, Y.M., Wagner, F., Hilker, T., Lyapustin, A.I., Wang, Y.J., Chave, J., Mottus, M., Aragao, L.E.O.C., Shimabukuro, Y., 2016. Consistency of vegetation index seasonality across the Amazon rainforest. *Int. J. Appl. Earth Obs. Geoinf.* 52, 42–53.
- Magney, T.S., Bowling, D.R., Logan, B.A., Grossmann, K., Stutz, J., Blanken, P.D., Burns, S.P., Cheng, R., Garcia, M.A., Kohler, P., Lopez, S., Parazoo, N.C., Racza, B., Schimel, D., Frankenberger, C., 2019. Mechanistic evidence for tracking the seasonality of photosynthesis with solar-induced fluorescence. *Proc. Natl. Acad. Sci. United States of America* 116, 11640–11645.
- Meng, R., Dennison, P.E., Zhao, F., Shendryk, I., Rickert, A., Hanavan, R.P., Cook, B.D., Serbin, S.P., 2018. Mapping canopy defoliation by herbivorous insects at the individual tree level using bi-temporal airborne imaging spectroscopy and LiDAR measurements. *Remote Sens. Environ.* 215, 170–183.
- Min, A., Guo, Z., Li, H., Peng, J., 2021. JMnet: joint metric neural network for hyperspectral unmixing. *IEEE Trans. Geosci. Remote Sens.* 60, 1–12.
- Mitchard, E.T.A., 2018. The tropical forest carbon cycle and climate change. *Nature* 559, 527–534.
- Mon, M.S., Mizoue, N., Htun, N.Z., Kajisa, T., Yoshida, S., 2012. Estimating forest canopy density of tropical mixed deciduous vegetation using Landsat data: a comparison of three classification approaches. *Int. J. Remote Sens.* 33, 1042–1057.
- Moon, M., Richardson, A.D., Friedl, M.A., 2021. Multiscale assessment of land surface phenology from harmonized Landsat 8 and Sentinel-2, PlanetScope, and PhenoCam imagery. *Remote Sens. Environ.* 266, 11271.
- Moore, C.E., Brown, T., Keenan, T.F., Duursma, R.A., van Dijk, A.I.J.M., Beringer, J., Culvenor, D., Evans, B., Huete, A., Hutley, L.B., Maier, S., Restrepo-Coupe, N., Sonnentag, O., Specht, A., Taylor, J.R., van Gorsel, E., Liddell, M.J., 2016. Reviews and syntheses: Australian vegetation phenology: new insights from satellite remote sensing and digital repeat photography. *Biogeosciences* 13, 5085–5102.
- Morellato, L.P.C., Alberton, B., Alvarado, S.T., Borges, B., Buisson, E., Camargo, M.G.G., Cancian, L.F., Carstensen, D.W., Escobar, D.F.E., Leite, P.T.P., Mendoza, I., Rocha, N., M.W.B., Soares, N.C., Silva, T.S.F., Staggemeier, V.G., Streher, A.S., Vargas, B.C., Peres, C.A., 2016. Linking plant phenology to conservation biology. *Biol. Conserv.* 195, 60–72.
- Morton, D.C., Nagol, J., Carabajal, C.C., Rosette, J., Palace, M., Cook, B.D., Vermote, E.F., Harding, D.J., North, P.R.J., 2014. Amazon forests maintain consistent canopy structure and greenness during the dry season. *Nature* 506, 221–224.
- Motohka, T., Nasahara, K.N., Oguma, H., Tsuchida, S., 2010. Applicability of green-red vegetation index for remote sensing of vegetation phenology. *Remote Sens.* 2, 2369–2387.
- Ozkan, S., Kaya, B., Akar, G.B., 2019. EndNet: sparse AutoEncoder network for endmember extraction and hyperspectral unmixing. *IEEE Trans. Geosci. Remote Sens.* 57, 482–496.
- Palsson, B., Ulfarsson, M.O., Sveinsson, J.R., 2021. Convolutional Autoencoder for spectral spatial hyperspectral unmixing. *IEEE Trans. Geosci. Remote Sens.* 59, 535–549.
- Panzou, G.J.L., Payolle, A., Jucker, T., Phillips, O.L., Bohlman, S., Banin, L.F., Lewis, S.L., Affum-Baffoe, K., Alves, L.F., Antin, C., Arets, E., Arroyo, L., Baker, T.R., Barbier, N., Beeckman, H., Berger, U., Bocko, Y.E., Bongers, F., Bowers, S., Brade, T., Brondum, E.S., Chantrain, A., Chave, J., Compaore, H., Coomes, D., Diallo, A., Dias, A.S., Dimobe, K., Djagbletey, G.D., Domingues, T., Doucet, J.L., Drouet, T., Forni, E., Godlee, J.L., Goodman, R.C., Gourlet-Fleury, S., Hien, F., Iida, Y., Ilondea, B.A., Muledi, J.I., Jacques, P., Kuyah, S., Lopez-Portillo, J., Loumeto, J.J., Marimon, B., Marimon, B.S., Mensah, S., Mitchard, E.T.A., Moncrieff, G.R., Narayanan, A., O'Brien, S.T., Ouedraogo, K., Palace, M.W., Pelissier, R., Ploton, P., Poorter, L., Ryan, C.M., Saiz, G., Santos, K., Schlund, M., Sellan, G., Sonke, B., Sterck, F., Thibaut, Q., Van Hoef, Y., Veenendaal, E., Vovides, A.G., Xu, Y.Z., Yao, T., L., Feldpausch, T.R., Kerkhoff, A., 2021. Pantropical variability in tree crown allometry. *Glob. Ecol. Biogeogr.* 30, 459–475.
- Park, J.Y., Muller-Landau, H.C., Lichstein, J.W., Rifai, S.W., Dandois, J.P., Bohlman, S.A., 2019. Quantifying leaf phenology of individual trees and species in a tropical forest using unmanned aerial vehicle (UAV) images. *Remote Sens.* 11 <https://doi.org/10.3390/rs11131534>.
- Pastorello, G., Trotta, C., Canfora, E., Chu, H.S., Christianson, D., Cheah, Y.W., Poindexter, C., Chen, J.Q., Elbashandy, A., Humphrey, M., Isaac, P., Polidori, D., Ribeca, A., van Ingen, C., Zhang, L.M., Amiro, B., Ammann, C., Arain, M.A., Ardo, J., Arkebauer, T., Arndt, S.K., Arriga, N., Aubinet, M., Aurela, M., Baldocchi, D., Barr, A., Beamesderfer, E., Marchesini, L.B., Bergeron, O., Beringer, J., Bernhofer, C., Berweiller, D., Billesbach, D., Black, T.A., Blanken, P.D., Bohrer, G., Boike, J., Bolstad, P.V., Bonal, D., Bonnefond, J.M., Bowling, D.R., Bracho, R., Brodeur, J., Brummer, C., Buchmann, N., Burban, B., Burns, S.P., Buisse, P., Cale, P., Cavagna, M., Cellier, P., Chen, S.P., Chini, I., Christensen, T.R., Cleverly, J., Collatiti, A., Consalvo, C., Cook, B.D., Cook, D., Coursolle, C., Cremonese, E., Curtis, P.S., D'Andrea, E., da Rocha, H., Dai, X.Q., Davis, K.J., De Cinti, B., de Grandcourt, A., De Ligne, A., De Oliveira, R.C., Delipierre, N., Desai, A.R., Di Bella, C., M., di Tommasi, P., Dolman, H., Domingo, F., Dong, G., Dore, S., Duce, P., Dufrene, E., Dunn, A., Dusek, J., Eamus, D., Eichelmann, U., Elkhidir, H.A.M., Eugster, W., Ewenz, C.M., Ewers, B., Famulari, D., Fares, S., Feigenwinter, I., Feitz, A., Fenstolt, R., Filippa, G., Fischer, M., Frank, J., Galvagno, M., Gharun, M., Gianelle, D., Gielen, B., Gioli, B., Gitelson, A., Goded, I., Goeckede, M., Goldstein, A., H., Gough, C.M., Goulden, M.L., Graf, A., Griebel, A., Gruening, C., Grunwald, T., Hammerle, A., Han, S.J., Han, X.G., Hansen, B.U., Hanson, C., Hatakka, J., He, Y.T., Hehn, M., Heinesch, B., Hinko-Najera, N., Hortnagl, L., Hutley, L., Ibrom, A., Ikawa, H., Jackowicz-Korczynski, M., Janous, D., Jans, W., Jassal, R., Jiang, S.C., Kato, T., Khomik, M., Klatt, J., Knoll, A., Knox, S., Kobayashi, H., Koerber, G., Kolle, O., Kosugi, Y., Kotani, A., Kowalski, A., Kruitj, B., Kurbatova, J., Kutsch, W.L., Kwon, H., Launiainen, S., Laurila, T., Law, B., Leuning, R., Li, Y.N., Liddell, M.,

- Limousin, J.M., Lion, M., Liska, A.J., Lohila, A., Lopez-Ballesteros, A., Lopez-Blanco, E., Loubet, B., Loustau, D., Lucas-Moffat, A., Luers, J., Ma, S.Y., Macfarlane, C., Magliulo, V., Maier, R., Mammarella, I., Manca, G., Marcolla, B., Margolis, H.A., Marras, S., Massman, W., Mastepanov, M., Matamala, R., Matthes, J.H., Mazzenga, F., McCaughey, H., McHugh, I., McMillan, A.M.S., Merbold, L., Meyer, W., Meyers, T., Miller, S.D., Minerbi, S., Moderow, U., Monson, R.K., Montagnani, L., Moore, C.E., Moors, E., Moreaux, V., Moureaux, C., Munger, J.W., Nakai, T., Neirynck, J., Nesic, Z., Nicolini, G., Noormets, A., Northwood, M., Nosetto, M., Nouvellon, Y., Novick, K., Oechel, W., Olesen, J.E., Ourcival, J.M., Papuga, S.A., Parmentier, F.J., Paul-Limoges, E., Pavelka, 2020. The FLUXNET2015 dataset and the ONEFlux processing pipeline for eddy covariance data. In: Peichl, M., Pendall, E., Phillips, R.P., Pilegaard, K., Pirk, N., Posse, G., Powell, T., Prasse, H., Prober, S.M., Rambal, S., Rannik, U., Raz-Yaseef, N., Reed, D., de Dios, V.R., Restrepo-Coupe, N., Reverter, B.R., Roland, M., Sabbatini, S., Sachs, T., Saleska, S.R., Sanchez-Canete, E.P., Sanchez-Mejia, Z.M. (Eds.), Scientific Data 7 (1), 1–27.
- Pau, S., Okamoto, D.K., Calderon, O., Wright, S.J., 2018. Long-term increases in tropical flowering activity across growth forms in response to rising CO<sub>2</sub> and climate change. *Glob. Chang. Biol.* 24, 2105–2116.
- Perez, A., Lopez, F., Benloch, J., Christensen, S., 2000. Colour and shape analysis techniques for weed detection in cereal fields. *Comput. Electron. Agric.* 25, 197–212.
- Planet, 2022. Planet Imagery Product Specification [WWW Document]. In (accessed 05 March 2022). [https://assets.planet.com/docs/Planet\\_Combined\\_Imagery\\_Product\\_Specs\\_letter\\_screen.pdf](https://assets.planet.com/docs/Planet_Combined_Imagery_Product_Specs_letter_screen.pdf).
- Qu, Y., Qi, H.R., 2019. uDAS: an untied denoising autoencoder with sparsity for spectral unmixing. *IEEE Trans. Geosci. Remote Sens.* 57, 1698–1712.
- Rasp, S., Pritchard, M.S., Gentine, P., 2018. Deep learning to represent subgrid processes in climate models. *Proc. Natl Acad. Sci. United States of America* 115, 9684–9689.
- Read, J.S., Jia, X.W., Willard, J., Applng, A.P., Zwart, J.A., Oliver, S.K., Karpatne, A., Hansen, G.J.A., Hanson, P.C., Watkins, W., Steinbach, M., Kumar, V., 2019. Process-guided deep learning predictions of lake water temperature. *Water Resour. Res.* 55, 9173–9190.
- Reich, P.B., 1995. Phenology of tropical forests - patterns, causes, and consequences. *Can. J. Botany-Revue Canadienne Botanique* 73, 164–174.
- Reich, P.B., Uhl, C., Walters, M.B., Prugh, L., Ellsworth, D.S., 2004. Leaf demography and phenology in Amazonian rain forest: a census of 40 000 leaves of 23 tree species. *Ecol. Monogr.* 74, 3–23.
- Reichstein, M., Camps-Valls, G., Stevens, B., Jung, M., Denzler, J., Carvalhais, N., Prabhat, 2019. Deep learning and process understanding for data-driven Earth system science. *Nature* 566, 195–204.
- Renner, S.S., Zohner, C.M., 2018. Climate change and phenological mismatch in trophic interactions among plants, insects, and vertebrates. *Annu. Rev. Ecol. Evol. Syst.* 49 (49), 165–182.
- Restrepo-Coupe, N., Levine, N.M., Christoffersen, B.O., Albert, L.P., Wu, J., Costa, M.H., Galbraith, D., Imbuzeiro, H., Martins, G., da Araujo, A.C., Malhi, Y.S., Zeng, X.B., Moorcroft, P., Saleska, S.R., 2017. Do dynamic global vegetation models capture the seasonality of carbon fluxes in the Amazon basin? A data-model intercomparison. *Glob. Chang. Biol.* 23, 191–208.
- Rouse, J.W., Haas, R.H., Schell, J.A., Deering, D.W., 1974. Monitoring vegetation systems in the Great Plains with ERTS. NASA Special Publication 351, 309.
- Ryu, J.Y., Kim, H.U., Lee, S.Y., 2019. Deep learning enables high-quality and high-throughput prediction of enzyme commission numbers. *Proc. Natl. Acad. Sci. United States of America* 116, 13996–14001.
- Saatchi, S.S., Harris, N.L., Brown, S., Lefsky, M., Mitchard, E.T.A., Salas, W., Zutta, B.R., Buermann, W., Lewis, S.L., Hagen, S., Petrova, S., White, L., Silman, M., Morel, A., 2011. Benchmark map of forest carbon stocks in tropical regions across three continents. *Proc. Natl. Acad. Sci. United States of America* 108, 9899–9904.
- Saleska, S.R., Wu, J., Guan, K.Y., Araujo, A.C., Huete, A., Nobre, A.D., Restrepo-Coupe, N., 2016. Dry-season greening of Amazon forests. *Nature* 531, E4–E5.
- Satake, A., Nagahama, A., Sasaki, E., 2022. A cross-scale approach to unravel the molecular basis of plant phenology in temperate and tropical climates. *New Phytol.* 233, 2340–2353.
- Schaaf, C.B., Gao, F., Strahler, A.H., Lucht, W., Li, X.W., Tsang, T., Strugnell, N.C., Zhang, X.Y., Jin, Y.F., Muller, J.P., Lewis, P., Barnsley, M., Hobson, P., Disney, M., Roberts, G., Dunderdale, M., Doll, C., d'Entremont, R.P., Hu, B.X., Liang, S.L., Privette, J.L., Roy, D., 2002. First operational BRDF, albedo nadir reflectance products from MODIS. *Remote Sens. Environ.* 83, 135–148.
- Shimabukuro, Y.E., Smith, J.A., 1991. The least-squares mixing models to generate fraction images derived from remote-sensing multispectral data. *IEEE Trans. Geosci. Remote Sens.* 29, 16–20.
- Somers, B., Asner, G.P., Tits, L., Coppin, P., 2011. Endmember variability in spectral mixture analysis: a review. *Remote Sens. Environ.* 115, 1603–1616.
- Song, G.Q., Wu, S.B., Lee, C.K.F., Serbin, S.P., Wolfe, B.T., Ng, M.K., Ely, K.S., Bogonovich, M., Wang, J., Lin, Z.Y., Saleska, S., Nelson, B.W., Rogers, A., Wu, J., 2022. Monitoring leaf phenology in moist tropical forests by applying a superpixel-based deep learning method to time-series images of tree canopies. *ISPRS J. Photogramm. Remote Sens.* 183, 19–33.
- Souza, C., Firestone, L., Silva, L.M., Roberts, D., 2003. Mapping forest degradation in the eastern Amazon from SPOT 4 through spectral mixture models. *Remote Sens. Environ.* 87, 494–506.
- Souza, C.M., Roberts, D.A., Cochrane, M.A., 2005. Combining spectral and spatial information to map canopy damage from selective logging and forest fires. *Remote Sens. Environ.* 98, 329–343.
- Su, Y.C., Li, J., Plaza, A., Marinoni, A., Gamba, P., Chakravortty, S., 2019. DAEN: deep Autoencoder networks for hyperspectral unmixing. *IEEE Trans. Geosci. Remote Sens.* 57, 4309–4321.
- Sulla-Menashe, D., Gray, J.M., Abercrombie, S.P., Friedl, M.A., 2019. Hierarchical mapping of annual global land cover 2001 to present: the MODIS collection 6 land cover product. *Remote Sens. Environ.* 222, 183–194.
- Sun, G.Y., Chen, X.L., Jia, X.P., Yao, Y.J., Wang, Z.J., 2016. Combinational Build-Up Index (CBI) for effective impervious surface mapping in urban areas. *IEEE J. Select. Top. Appl. Earth Observ. Remote Sens.* 9, 2081–2092.
- Torgbor, B.A., Rahman, M.M., Robson, A., Brinkhoff, J., Khan, A., 2022. Assessing the potential of Sentinel-2 derived vegetation indices to retrieve phenological stages of Mango in Ghana. *Horticultriae 8.* <https://doi.org/10.3390/horticultriae8010011>.
- Vanschaik, C.P., Terborgh, J.W., Wright, S.J., 1993. The phenology of tropical forests - adaptive significance and consequences for primary consumers. *Annu. Rev. Ecol. Syst.* 24, 353–377.
- Wagner, F.H., Herault, B., Rossi, V., Hilker, T., Maeda, E.E., Sanchez, A., Lyapustin, A.I., Galvao, L.S., Wang, Y.J., Aragao, L.E.O.C., 2017. Climate drivers of the Amazon forest greening. *Plos One* 12.
- Wang, J., Yang, D.D., Chen, S.L., Zhu, X.L., Wu, S.B., Bogonovich, M., Guo, Z.F., Zhu, Z., Wu, J., 2021. Automatic cloud and cloud shadow detection in tropical areas for PlanetScope satellite images. *Remote Sens. Environ.* 264 <https://doi.org/10.1016/j.rse.2021.112604>.
- Wang, J., Yang, D.D., Detto, M., Nelson, B.W., Chen, M., Guan, K.Y., Wu, S.B., Yan, Z.B., Wu, J., 2020. Multi-scale integration of satellite remote sensing improves characterization of dry-season green-up in an Amazon tropical evergreen forest. *Remote Sens. Environ.* 246 <https://doi.org/10.1016/j.rse.2020.111865>.
- Wei, D.D., Fuentes, J.D., Gerken, T., Chamecki, M., Trowbridge, A.M., Stoy, P.C., Katul, G.G., Fisch, G., Acevedo, O., Manzi, A., von Randow, C., dos Santo, R.M.N., 2018. Environmental and biological controls on seasonal patterns of isoprene above a rain forest in Central Amazonia. *Agric. For. Meteorol.* 256, 391–406.
- Wright, J.S., Fu, R., Worden, J.R., Chakraborty, S., Clinton, N.E., Risi, C., Sun, Y., Yin, L., 2017. Rainforest-initiated wet season onset over the southern Amazon. *Proc. Natl. Acad. Sci. U.S.A* 114, 8481–8486.
- Wu, J., Albert, L.P., Lopes, A.P., Restrepo-Coupe, N., Hayek, M., Wiedemann, K.T., Guan, K.Y., Stark, S.C., Christoffersen, B., Prohaska, N., Tavares, J.V., Marostica, S., Kobayashi, H., Ferreira, M.L., Campos, K.S., da Silva, R., Brando, P.M., Dye, D.G., Huxman, T.E., Huete, A.R., Nelson, B.W., Saleska, S.R., 2016. Leaf development and demography explain photosynthetic seasonality in Amazon evergreen forests. *Science* 351, 972–976.
- Wu, J., Kobayashi, H., Stark, S.C., Meng, R., Guan, K.Y., Tran, N.N., Gao, S.C., Yang, W., Restrepo-Coupe, N., Miura, T., Oliviera, R.C., Rogers, A., Dye, D.G., Nelson, B.W., Serbin, S.P., Huete, A.R., Saleska, S.R., 2018. Biological processes dominate seasonality of remotely sensed canopy greenness in an Amazon evergreen forest. *New Phytol.* 217, 1507–1520.
- Wu, S.B., Wang, J., Yan, Z.B., Song, G.Q., Chen, Y., Ma, Q., Deng, M.F., Wu, Y.T., Zhao, Y., Guo, Z.F., Xu, X.T., Yang, X., Su, Y.J., Liu, L.L., Wu, J., 2021. Monitoring tree-crown scale autumn leaf phenology in a temperate forest with an integration of PlanetScope and drone remote sensing observations. *ISPRS J. Photogramm. Remote Sens.* 171, 36–48.
- Xia, J.Y., Niu, S.L., Ciais, P., Janssens, I.A., Chen, J.Q., Ammann, C., Arain, A., Blancken, P.D., Cescatti, A., Bonal, D., Buchmann, N., Curtis, P.S., Chen, S.P., Dong, J.W., Flanagan, L.B., Frankenberg, C., Georgiadis, T., Gough, C.M., Hui, D.F., Kiely, G., Li, J.W., Lund, M., Magliulo, V., Marcolla, B., Merbold, L., Montagnani, L., Moors, E.J., Olesjen, J.E., Piao, S.L., Raschi, A., Rouspard, O., Suyker, A.E., Urbaniak, M., Vaccari, F.P., Varlagin, A., Vesala, T., Wilkinson, M., Weng, E., Wohlfahrt, G., Yan, L.M., Luo, Y.Q., 2015. Joint control of terrestrial gross primary productivity by plant phenology and physiology. *Proc. Natl. Acad. Sci. U.S.A.* 112, 2788–2793.
- Xu, X., Shi, Z.W., Pan, B., Li, X.L., 2019. A classification-based model for multi-objective hyperspectral sparse unmixing. *IEEE Trans. Geosci. Remote Sens.* 57, 9612–9625.
- Xu, X.T., Medvigy, D., Wright, S.J., Kitajima, K., Wu, J., Albert, L.P., Martins, G.A., Saleska, S.R., Pacala, S.W., 2017. Variations of leaf longevity in tropical moist forests predicted by a trait-driven carbon optimality model. *Ecol. Lett.* 20, 1097–1106.
- Xu, X.Y., Riley, W.J., Koven, C.D., Jia, G.S., Zhang, X.Y., 2020. Earlier leaf-out warms air in the north. *Nat. Clim. Chang.* 10, 370–375.
- Yan, D., Scott, R.L., Moore, D.J.P., Biederman, J.A., Smith, W.K., 2019. Understanding the relationship between vegetation greenness and productivity across dryland ecosystems through the integration of PhenoCam, satellite, and eddy covariance data. *Remote Sens. Environ.* 223, 50–62.
- Yang, X., Tang, J.W., Mustard, J.F., Lee, J.E., Rossini, M., Joiner, J., Munger, J.W., Kornfeld, A., Richardson, A.D., 2015. Solar-induced chlorophyll fluorescence that correlates with canopy photosynthesis on diurnal and seasonal scales in a temperate deciduous forest. *Geophys. Res. Lett.* 42, 2977–2987.
- Zare, A., Ho, K.C., 2014. Endmember variability in hyperspectral analysis. *IEEE Signal Process. Mag.* 31, 95–104.
- Zhang, X., Liu, L.Y., Chen, X.D., Gao, Y., Xie, S., Mi, J., 2021. GLC\_FCS30: global land-cover product with fine classification system at 30m using time-series Landsat imagery. *Earth Syst. Sci. Data* 13, 2753–2776.
- Zhang, X.Y., Liu, L.L., Liu, Y., Jayavelu, S., Wang, J.M., Moon, M., Henebry, G.M., Friedl, M.A., Schaaf, C.B., 2018. Generation and evaluation of the VIIRS land surface phenology product. *Remote Sens. Environ.* 216, 212–229.